Euro. Jnl of Applied Mathematics (2010), *vol.* 21, *pp.* 479–517. © Cambridge University Press 2010
doi:10.1017/S0956792510000197

Dynamic coupling between shallow-water sloshing and horizontal vehicle motion

HAMID ALEMI ARDAKANI and THOMAS J. BRIDGES

Department of Mathematics, University of Surrey, Guildford GU2 7XH, UK
emails: H.Alemiardakani@surrey.ac.uk & T.Bridges@surrey.ac.uk

(*Received 4 November 2009; revised 21 May 2010; accepted 26 May 2010; first published online 7 July 2010*)

The coupled motion between shallow-water sloshing in a moving vehicle and the vehicle dynamics is considered, with the vehicle dynamics restricted to horizontal motion. The paper is motivated by Cooker's experiments and theory for water waves in a suspended container. A new derivation of the coupled problem in the Eulerian fluid representation is given. However, it is found that transformation to a Lagrangian representation leads to a formulation which has nice properties for numerical simulation. In the Lagrangian representation, a simple and fast numerical algorithm with excellent energy conservation over long times, based on the Störmer–Verlet method, is implemented. Numerical simulations of the coupled dynamics in both the linear and non-linear case are presented.

1 Introduction

The effect of liquid sloshing on the dynamics and control of liquid transport, e.g. the terrestrial transport of liquids, oil and liquid natural gas in ships, and fuel in aviation and astrodynamics, has motivated a wide range of research. An indication of the breadth of research in this area is the book of Ibrahim [14] which cites over 2000 references.

The interest in this paper is in the dynamic coupling between shallow-water fluid sloshing and the motion of the transport vehicle. Examples of where dynamic coupling is of interest is the sloshing of water on the deck of fishing vessels [6], transport of liquid by robots [26, 27], motion planning for industrial control [10–12, 24], sloshing in automobile fuel tanks [4] and motion of water waves in a suspended container [8]. It is the last paper that motivates the present study.

In this paper, attention will be restricted to the case of horizontal motion only (for translation and rotation of the vessel coupled to shallow-water sloshing see [2]). Equations for this coupled problem have been derived by Cooker [8]. Let $q(t)$ be the horizontal position of the vessel, then the governing equations are

$$\begin{aligned} h_t + uh_x + hu_x &= 0, \\ u_t + uu_x + gh_x &= -\ddot{q}, \end{aligned} \tag{1.1}$$

on the interval $0 \leqslant x \leqslant L$ with

$$u(0,t) = u(L,t) = 0 \quad \text{for all} \quad t.$$

https://doi.org/10.1017/S0956792510000197 Published online by Cambridge University Press

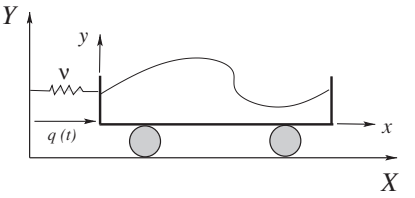


FIGURE 1. Schematic of a moving vehicle constrained by a spring force partially filled with fluid.

Here $u(x,t)$ is a representative horizontal fluid velocity relative to the non-inertial (x,y) frame attached to the vehicle, whereas $q(t)$ is the tank displacement relative to the inertial (X,Y) laboratory frame. A schematic is shown in Figure 1. The free surface is represented by the time-dependent curve $y=h(x,t)$.

The governing equation for $q(t)$ is Cooker's equation

$$m_v\ddot{q}+vq=\tfrac{1}{2}\rho g(h(L,t)^2-h(0,t)^2). \tag{1.2}$$

The coupling is non-local since the right-hand side of (1.2) can be interpreted as an integral

$$\tfrac{1}{2}\rho g(h(L,t)^2-h(0,t)^2)=\rho g\int_0^L hh_x\,\mathrm{d}x.$$

With an appropriate change of notation and change of reference frame, equation (1.2) is equation (9) in [8]. Here and throughout the paper ρ is the fluid density, which is taken to be constant. The fluid and vessel are assumed to have unit width. The mass of the dry vessel is denoted by m_v and $v>0$ is a spring constant. A new derivation of (1.1)–(1.2) identifying the key assumptions is given in Section 2.

When $q(t)$ is given, (1.2) is neglected and the shallow-water equations (1.1) are forced by the time-dependent function $\ddot{q}(t)$. This problem has been extensively studied (e.g. [7, 9, 16, 21, 22, 28]), and it has been shown to lead to very complicated motion. One measure of the difference with the coupled case is the role of energy. In the case of forced motion, the energy is not conserved

$$\frac{\mathrm{d}E}{\mathrm{d}t}=-\ddot{q}\int_0^L \rho hu\,\mathrm{d}x,$$

where

$$E(t)=\int_0^L \left(\tfrac{1}{2}\rho hu^2+\tfrac{1}{2}\rho gh^2\right)\mathrm{d}x.$$

On the other hand, the energy of the coupled problem is conserved: $\frac{\mathrm{d}E_c}{\mathrm{d}t}=0$ where

$$E_c(t)=\int_0^L \left(\tfrac{1}{2}\rho h(u+\dot{q})^2+\tfrac{1}{2}\rho gh^2\right)\mathrm{d}x+\tfrac{1}{2}m_v\dot{q}^2+\tfrac{1}{2}vq^2. \tag{1.3}$$

The last two terms in (1.3) are the kinetic and potential energy of the vehicle.

Previous work on the problem of coupled vehicle translation and sloshing includes [15, 19] where the coupled problem allowing for two-dimensional flow is studied. In [19] the linear coupled problem is considered, and in [15] asymptotic results are derived. In

https://doi.org/10.1017/S0956792510000197 Published online by Cambridge University Press

[8] the fluid is considered to be shallow, and a detailed study of the adjusted natural frequencies is presented and compared with experiments.

The aim of this paper is to develop a numerical method for the non-linear coupled system (1.1)–(1.2) and present simulations. Solving the coupled system numerically would appear on the face of it to be straightforward. The system (1.1) can be solved by a typical shallow-water equation solver of which there are many, and the vessel equation (1.2) is just a forced harmonic oscillator. However, the fact that the acceleration (rather than velocity or position) of the vessel appears in (1.1) and non-linear non-local coupling appears in (1.2) does present problems. At first we solved (1.1) using an implicit shallow-water equation solver. The scheme we used is the same one that is used in [1]. It is a very effective numerical scheme for the *forced* problem [1]. We coupled it with a standard fourth-order Runge–Kutta method for the vessel equation (1.2) and iteration was used to deal with the non-linearities. This coupled numerical scheme is effective for waves which come close to breaking because the implicit scheme has a dissipative interface. However, in order to model long-time oscillatory behaviour a scheme which conserves energy is of interest.

Re-thinking the problem led us to consider the Lagrangian particle path (LPP) formulation for the fluid. In computational fluid dynamics, the Eulerian fluid representation is preferred over the Lagrangian representation since mesh distortion can cause problems. However in one space dimension mesh distortion is not a problem. Indeed, the LPP representation of the equations takes an elegant and simple form. Let $x(a,t)$ be the position of a fluid particle, with $0 \leqslant a \leqslant L$ the reference space. Then $u = x_t$ and the two equations in (1.1) reduce to

$$\frac{\partial^2 x}{\partial t^2} + \frac{g}{x_a}\frac{\partial}{\partial a}\left(\frac{\chi}{x_a}\right) = -\ddot{q}. \tag{1.4}$$

Assuming non-degeneracy of the label map, $x_a \neq 0$, the wave profile is obtained from

$$h = \chi(a) x_a^{-1},$$

with $\chi(a) := hx_a|_{t=0}$ determined by the initial conditions. The equation for $q(t)$ in (1.2) remains the same with h expressed in terms of $x(a,t)$.

The LPP formulation has been extensively used for the analogous problem in acoustics (e.g. Seymour & Mortell [25] and followup work), when the piston at one end is moving, and in the analysis of shallow-water sloshing when one end of the vessel is moving (e.g. Cox *et al.* [9]). The main new feature here is the LPP formulation of the coupled problem, and the fact that the equations can be deduced from a variational principle.

The coupled LPP equations – equations (1.2) and (1.4) – are completely determined by the Euler–Lagrange equation of the Lagrangian[1] functional

$$\mathscr{L}(x,q) = \int_{t_1}^{t_2}\int_0^L \left(\frac{1}{2}(\dot{x}+\dot{q})^2 - \frac{1}{2}g\frac{\chi(a)}{x_a}\right)\rho\chi(a)\,\mathrm{d}a\,\mathrm{d}t + \int_{t_1}^{t_2}\left(\frac{1}{2}m_v\dot{q}^2 - \frac{1}{2}vq^2\right)\mathrm{d}t. \tag{1.5}$$

A derivation is given in Section 4.1. The advantage of the variational principle is that it is much easier to design a numerical scheme with good energy conservation properties. The

[1] Note that the word 'Lagrangian' is used in two distinct ways in this paragraph.

https://doi.org/10.1017/S0956792510000197 Published online by Cambridge University Press

Euler–Lagrange equations also have a Hamiltonian formulation. This structure suggests that a symplectic integrator can be used. In this paper, a variant of the Störmer–Verlet algorithm is used. This algorithm has excellent energy and momentum conservation properties [13, 18], and it is explicit.

Simulations are shown for both the linear and non-linear case. In the linear case, away from 'resonance' (see Section 5 for definition of resonance) an exact solution can be computed and comparison with the simulation shows excellent agreement. At resonance, simulations show distinctly non-harmonic motion. The non-linear simulations show quite regular behaviour over a range of parameter values, although the initial conditions are restricted to a quiescent fluid. The initial momentum or position of the vehicle is prescribed, the latter being the initial condition in Cooker's experiments [8]. A numerical simulation with $v = 0$ is also presented showing vehicle drift coupled with vehicle 'wobble'.

2 Governing equations

There are two frames of reference. The spatial (inertial) frame has coordinates $\mathbf{X} = (X, Y)$ and the body frame has coordinates $\mathbf{x} = (x, y)$. The whole system has a uniform translation, denoted $q(t)$, in the $x-$direction; hence

$$X = x + q \quad \text{and} \quad Y = y.$$

The vessel is a rigid body and the body frame is attached as shown in Figure 1. The fluid occupies the region

$$0 \leqslant y \leqslant h(x,t) \quad \text{with} \quad 0 \leqslant x \leqslant L.$$

Assuming inviscid flow with velocity field $(u(x,y,t), v(x,y,t))$ and pressure field $p(x,y,t)$, the Eulerian representation of the momentum equations for the fluid in the vessel relative to the body coordinate system is

$$\frac{\mathrm{D}u}{\mathrm{D}t} + \frac{1}{\rho}\frac{\partial p}{\partial x} = -\ddot{q} \quad \text{and} \quad \frac{\mathrm{D}v}{\mathrm{D}t} + \frac{1}{\rho}\frac{\partial p}{\partial y} = -g, \tag{2.1}$$

where $g > 0$ is the gravitational constant and $\frac{\mathrm{D}u}{\mathrm{D}t} := \frac{\partial u}{\partial t} + u\frac{\partial u}{\partial x} + v\frac{\partial u}{\partial y}$. Conservation of mass in the Eulerian representation, relative to the body frame, takes the usual form

$$u_x + v_y = 0. \tag{2.2}$$

The boundary conditions at the vessel walls are

$$u = 0 \quad \text{at} \quad x = 0 \quad \text{and} \quad x = L, \quad v = 0 \quad \text{at} \quad y = 0. \tag{2.3}$$

Neglecting surface tension, the boundary conditions at the free surface are

$$p = 0 \quad \text{and} \quad h_t + uh_x = v \quad \text{at} \quad y = h(x,t). \tag{2.4}$$

The *surface velocity field* is defined by

$$U(x,t) := u(x, h(x,t), t) \quad \text{and} \quad V(x,t) := v(x, h(x,t), t). \tag{2.5}$$

https://doi.org/10.1017/S0956792510000197 Published online by Cambridge University Press

To derive an equation for the horizontal surface velocity field, first note that

$$U_t + UU_x = (u_t + u_y h_t + u(u_x + u_y h_x)) = \frac{\mathrm{D}u}{\mathrm{D}t} \qquad \text{at } y = h(x,t),$$

using the definition (2.5) and the kinematic condition (2.4). Hence evaluation of the horizontal component of the momentum equation (2.1) at the free surface gives

$$U_t + UU_x + \frac{1}{\rho} p_x = -\ddot{q} \qquad \text{at } y = h(x,t). \tag{2.6}$$

But, remarkably,

$$\frac{\partial p}{\partial x} = \rho \left(g + \frac{\mathrm{D}v}{\mathrm{D}t} \right) h_x \qquad \text{at } y = h(x,t), \tag{2.7}$$

where $\frac{\mathrm{D}v}{\mathrm{D}t}$ is the Lagrangian vertical acceleration. This latter identity follows from integration of the vertical momentum equation in (2.1):

$$p(x,y,t) = \rho g(h-y) + \rho \int_y^h \frac{\mathrm{D}v}{\mathrm{D}t}\, \mathrm{d}s,$$

differentiating with respect to x and taking the limit $y \to h$. A detailed derivation of the identity (2.7) and its generalizations is given in [1, 5].

Combining (2.6) with (2.7) shows that the horizontal surface velocity field satisfies the exact equation

$$U_t + UU_x + \left(g + \frac{\mathrm{D}v}{\mathrm{D}t} \right) h_x = -\ddot{q} \qquad \text{at } y = h(x,t). \tag{2.8}$$

To derive an equation for $h(x,t)$, start with the kinematic condition

$$h_t + Uh_x = V,$$

and recast it into the form

$$h_t + (hU)_x = V + hU_x. \tag{2.9}$$

This equation is exact. In order to reduce to a shallow-water approximation, it must be argued that the right-hand side is small, and this is argued in Section 3.

2.1 Vehicle motion

To derive Cooker's equation (1.2), start with Newton's second law for the coupled system. If the only force acting on the vehicle is the spring force, then Newton's second law gives

$$\frac{\mathrm{d}}{\mathrm{d}t} \left(\int_0^L \int_0^h \rho u \, \mathrm{d}y \, \mathrm{d}x + (m_f + m_v)\dot{q} \right) = -vq, \tag{2.10}$$

where m_f is the mass of the fluid:

$$m_f = \int_0^L \int_0^h \rho \, \mathrm{d}y \, \mathrm{d}x = \rho h_0 L \quad \text{with} \quad h_0 = \frac{1}{L} \int_0^L h(x,t)\, \mathrm{d}x.$$

https://doi.org/10.1017/S0956792510000197 Published online by Cambridge University Press

The still water level h_0 is independent of time because $\int_0^L h(x,t)\,\mathrm{d}x$ is a constant of the motion (for both the two-dimensional problem and the shallow-water approximation). A more familiar form of the motion equation, involving the pressure, can be derived using the governing equations. Differentiating the total fluid momentum and using the horizontal momentum equation in (2.1):

$$\begin{aligned}\frac{\mathrm{d}}{\mathrm{d}t}\int_0^L\int_0^h \rho u\,\mathrm{d}y\,\mathrm{d}x &= \int_0^L\int_0^h \rho\frac{\mathrm{D}u}{\mathrm{D}t}\,\mathrm{d}y\,\mathrm{d}x\\ &= \int_0^L\int_0^h (-p_x-\rho\ddot{q})\,\mathrm{d}y\,\mathrm{d}x\\ &= -m_f\ddot{q}-\int_0^L\left(\frac{\partial}{\partial x}\int_0^h p\,\mathrm{d}y\right)\mathrm{d}x+\int_0^L p(x,h(x,t),t)h_x\,\mathrm{d}x\\ &= -m_f\ddot{q}-\int_0^h p\,\mathrm{d}y\Big|_{x=0}^{x=L},\end{aligned}$$

where Reynold's transport theorem is used in the first line and the boundary condition $p=0$ at $y=h(x,t)$ is used in the last line. Combining this equation with (2.10) gives

$$m_v\ddot{q}+vq=\int_0^h p(L,y,t)\,\mathrm{d}y-\int_0^h p(0,y,t)\,\mathrm{d}y.$$

This latter equation is the one most often used in the literature (e.g. equations (3)–(4) in [15] and equation (27) in [19]). However, we will find that it is the form (2.10) that will be useful in the numerical simulation.

To construct a shallow-water approximation for the coupled motion, first note that

$$\int_0^L\int_0^h \rho u\,\mathrm{d}y\,\mathrm{d}x=\int_0^L \rho hU\,\mathrm{d}x-\int_0^L\int_0^h \rho y u_y\,\mathrm{d}y\,\mathrm{d}x.$$

Substitute into the governing equation (2.10)

$$\frac{\mathrm{d}}{\mathrm{d}t}\left(\int_0^L \rho hU\,\mathrm{d}x+(m_f+m_v)\dot{q}\right)+vq=\frac{\mathrm{d}}{\mathrm{d}t}\int_0^L\int_0^h \rho y u_y\,\mathrm{d}y\,\mathrm{d}x, \tag{2.11}$$

3 Coupled shallow-water sloshing and vehicle motion

The exact equations for (h,U,q) are

$$\begin{aligned} U_t+UU_x+gh_x+\ddot{q} &= -\frac{\mathrm{D}v}{\mathrm{D}t}h_x \quad \text{at} \quad y=h(x,t)\\ h_t+(hU)_x &= V+hU_x,\\ \frac{\mathrm{d}}{\mathrm{d}t}\left(\int_0^L \rho hU\,\mathrm{d}x+(m_f+m_v)\dot{q}\right)+vq &= \frac{\mathrm{d}}{\mathrm{d}t}\int_0^L\int_0^h \rho y u_y\,\mathrm{d}y\,\mathrm{d}x.\end{aligned} \tag{3.1}$$

This set of equations is not closed since the right-hand sides contain terms involving $v(x,y,t)$ and $u(x,y,t)$. A closed set of equations for $h(x,t)$, $U(x,t)$ and $q(t)$ is obtained by

https://doi.org/10.1017/S0956792510000197 Published online by Cambridge University Press

neglecting the right-hand sides of (3.1). The principal assumptions are

$$\left|\frac{\mathrm{D}v}{\mathrm{D}t}\,h_x\right| \ll 1 \quad \text{when evaluated at} \quad y = h(x,t), \tag{3.2}$$

and

$$|V + hU_x| \ll 1 \quad \text{and} \quad \left|\frac{\mathrm{d}}{\mathrm{d}t}\int_0^L\int_0^h \rho y u_y \,\mathrm{d}y\,\mathrm{d}x\right| \ll 1. \tag{3.3}$$

All three assumptions are familiar from shallow-water theory. The first essentially requires that the Lagrangian vertical acceleration at the free surface be small. This condition is a special case of the usual assumption in shallow water theory that the Lagrangian vertical acceleration be small *everywhere* in the flow [17]. The second and third assumptions in (3.3) are special cases of the usual assumptions in shallow-water theory that the horizontal velocity is independent of y (hence $u_y = 0$) and the vertical velocity is a linear function of y [17]: assuming $u(x,y,t)$ is independent of y in (2.2) gives $v + yu_x = 0$ and evaluation at the free surface is consistent with the first assumption in (3.3).

With these assumptions, the shallow-water equations (SWEs) for the fluid are

$$\begin{aligned} h_t + hU_x + Uh_x &= 0, \\ U_t + UU_x + gh_x &= -\ddot{q}, \end{aligned} \tag{3.4}$$

coupled to

$$\frac{\mathrm{d}}{\mathrm{d}t}\left(\int_0^L \rho h U \,\mathrm{d}x + (m_f + m_v)\dot{q}\right) + vq = 0. \tag{3.5}$$

This completes the derivation of (1.1)–(1.2). To see that (3.5) is the same as Cooker's equation (1.2), use (3.4) to transform

$$\begin{aligned} \frac{\mathrm{d}}{\mathrm{d}t}\int_0^L \rho h U \,\mathrm{d}x &= \int_0^L \rho(h_t U + hU_t)\,\mathrm{d}x \\ &= -\int_0^L \rho\left[(hU^2)_x + ghh_x + h\ddot{q})\right]\mathrm{d}x \\ &= -m_f\ddot{q} - \int_0^L \rho g h h_x \,\mathrm{d}x. \end{aligned}$$

Substitution into (3.5) then gives (1.2).

Cooker [8] shows that the linear problem has two important dimensionless parameters

$$R = \frac{m_v}{m_f} \quad \text{and} \quad G = \frac{vL^2}{4gh_0 m_f}, \tag{3.6}$$

and they are equally important for the non-linear problem. The other key dimensionless parameter is the fluid aspect ratio h_0/L.

The use of the velocity at the free surface $U(x,t)$ is one possible choice for the one-dimensional horizontal velocity. Another interesting choice is the vertical average of the two-dimensional horizontal velocity. This choice leads to the same equations (1.1)–(1.2) but with different assumptions. The implications of this last choice are explored in Appendix A.

https://doi.org/10.1017/S0956792510000197 Published online by Cambridge University Press

4 Lagrangian particle path formulation of the SWEs

To derive the LPP form of the equations consider the mapping

$$(t,a)\mapsto(t,x(a,t))\quad\text{with}\quad 0\leqslant a\leqslant L,\quad t\geqslant 0.$$

Assuming non-degeneracy ($x_a\neq 0$) the derivatives in (1.1) are mapped to

$$\frac{\partial}{\partial t}\mapsto\frac{\partial}{\partial t}-x_t x_a^{-1}\frac{\partial}{\partial a}\quad\text{and}\quad\frac{\partial}{\partial x}\mapsto x_a^{-1}\frac{\partial}{\partial a}.$$

Substitute into (3.4)

$$\begin{aligned}h_t-x_t x_a^{-1}h_a+Ux_a^{-1}h_a+hx_a^{-1}U_a&=0,\\ U_t-x_t x_a^{-1}U_a+Ux_a^{-1}U_a+gx_a^{-1}h_a&=-\ddot{q}.\end{aligned}$$

Setting $U=x_t$ and multiplying the first equation by x_a simplifies these equations to

$$\begin{aligned}x_a h_t+hx_{at}&=0,\\ x_{tt}+gx_a^{-1}h_a&=-\ddot{q}.\end{aligned}\tag{4.1}$$

The first equation gives that hx_a is independent of time and so

$$hx_a=hx_a\Big|_{t=0},\quad\text{hence define}\quad\chi(a):=hx_a|_{t=0}.$$

The second equation of (4.1) then reduces to

$$\frac{\partial^2 x}{\partial t^2}+\frac{g}{x_a}\frac{\partial}{\partial a}\left(\frac{\chi}{x_a}\right)=-\ddot{q}.$$

This completes the derivation of (1.4). Equation (1.4) can also be expressed in conservation law form

$$\frac{\partial}{\partial t}((U+\dot{q})\chi)+\frac{\partial}{\partial a}\left(\frac{1}{2}gh^2\right)=0.$$

The equation for the vessel motion also needs to be transformed to the LPP setting. The total momentum transforms as

$$\int_0^L\rho hU\,\mathrm{d}x=\int_0^L\rho hUx_a\,\mathrm{d}a=\int_0^L U\,\rho\chi(a)\,\mathrm{d}a=\frac{\mathrm{d}}{\mathrm{d}t}\int_0^L x(a,t)\,\rho\chi(a)\,\mathrm{d}a.$$

Therefore Newton's law for the vessel motion in the LPP setting is

$$\frac{\mathrm{d}^2}{\mathrm{d}t^2}\left(\int_0^L x(a,t)\rho\chi(a)\,\mathrm{d}a+(m_v+m_f)q(t)\right)+vq(t)=0,\tag{4.2}$$

and the LPP version of Cooker's equation is

$$m_v\ddot{q}+vq=\frac{1}{2}m_f\frac{g}{h_0L}\frac{\chi(a)^2}{x_a^2}\Big|_{a=0}^{a=L}.$$

https://doi.org/10.1017/S0956792510000197 Published online by Cambridge University Press

The first term in the brackets in (4.2) is proportional to the horizontal centre of mass (see Appendix C for derivation) and so the vehicle equation can be expressed in the form

$$\frac{\mathrm{d}^2}{\mathrm{d}t^2}\left(\text{c.m.} + (1+R)q(t)\right) = -\frac{v}{m_f}q(t). \tag{4.3}$$

When the spring force is absent the position of the vehicle is completely determined by the position of the centre of mass of the fluid and the initial conditions.

4.1 Lagrangian variational principle for the coupled problem

The coupled equations for $x(a,t)$ and $q(t)$ can be determined from a variational principle using the Lagrangian functional introduced in (1.5).

Taking the first variation of the Lagrangian action (1.5) with respect to q gives

$$\begin{aligned}\left.\frac{\mathrm{d}}{\mathrm{d}s}\right|_{s=0}\mathscr{L}(x, q+s\widehat{q}) &= \int_{t_1}^{t_2}\widehat{q}_t\int_0^L (x_t+q_t)\,\rho\chi(a)\,\mathrm{d}a\,\mathrm{d}t + \int_{t_1}^{t_2}(m_v\widehat{q}_t q_t - v\widehat{q}q)\,\mathrm{d}t\\ &= \int_{t_1}^{t_2}\widehat{q}_t\left[\int_0^L x_t\,\rho\chi(a)\,\mathrm{d}a + (m_f+m_v)q_t\right]\mathrm{d}t - \int_{t_1}^{t_2} v\widehat{q}q\,\mathrm{d}t.\end{aligned}$$

Integrating by parts and using fixed endpoint conditions on the variations $\widehat{q}$ gives the equation for q in (4.2).

Now take the first variation of the action integral (1.5) with respect to x,

$$\begin{aligned}\left.\frac{\mathrm{d}}{\mathrm{d}s}\right|_{s=0}\mathscr{L}(x+s\widehat{x}, q) &= \int_{t_1}^{t_2}\int_0^L\left((x_t+q_t)\,\widehat{x}_t + \frac{g\chi(a)}{2x_a^2}\widehat{x}_a\right)\rho\chi(a)\,\mathrm{d}a\,\mathrm{d}t\\ &= \int_{t_1}^{t_2}\int_0^L\left(-x_{tt} - q_{tt} - \frac{g\chi_a}{x_a^2} + \frac{g\chi x_{aa}}{x_a^3}\right)\widehat{x}\rho\chi(a)\,\mathrm{d}a\,\mathrm{d}t,\end{aligned}$$

where integration by parts has been used to obtain the second equation, with boundary terms neglected. Setting this expression to zero recovers the LPP equation for $x(a,t)$ in (1.4).

We have also found a variational principle for the Eulerian form of the coupled equations (see Appendix B), but it is (so far) less useful for constructing a numerical scheme.

4.2 Hamiltonian formulation

The coupled system can also be expressed in Hamiltonian form with canonical variables (q, x, p, w). The momentum variables are

$$\begin{aligned}w(a,t) &= x_t(a,t) + q_t(t),\\ p(t) &= (m_v+m_f)q_t(t) + \int_0^L x_t(a,t)\rho\chi(a)\,\mathrm{d}a,\\ &= m_v q_t(t) + \int_0^L w(a,t)\rho\chi(a)\,\mathrm{d}a.\end{aligned} \tag{4.4}$$

https://doi.org/10.1017/S0956792510000197 Published online by Cambridge University Press

It is a mixed system in the sense that $x(a,t), w(a,t)$ depend on a as well as t but $q(t), p(t)$ are dependent on t only. The Hamiltonian formulation is derived by taking the Legendre transform of $\mathscr{L}$. The Hamiltonian functional is

$$\begin{aligned}\mathscr{H}(x,q,w,p) = \int_0^L \frac{1}{2}w^2\rho\chi\,\mathrm{d}a - \frac{1}{m_v}p\int_0^L w\rho\chi\,\mathrm{d}a + \frac{1}{2}\frac{1}{m_v}p^2 \\ + \frac{1}{2}\frac{1}{m_v}\left(\int_0^L w\rho\chi\,\mathrm{d}a\right)^2 + \frac{1}{2}vq^2 + \int_0^L \frac{1}{2}\rho g\frac{\chi^2}{x_a}\,\mathrm{d}a.\end{aligned} \tag{4.5}$$

The governing equations in Hamiltonian form are

$$\begin{aligned}-\dot{w} &= \frac{\delta\mathscr{H}}{\delta x} = \frac{g\chi_a}{x_a^2} - \frac{g\chi}{x_a^3}x_{aa},\\ -\dot{p} &= \frac{\delta\mathscr{H}}{\delta q} = vq,\\ \dot{x} &= \frac{\delta\mathscr{H}}{\delta w} = w - \frac{1}{m_v}p + \frac{1}{m_v}\int_0^L w\,\rho\chi(a)\,\mathrm{d}a,\\ \dot{q} &= \frac{\delta\mathscr{H}}{\delta p} = \frac{1}{m_v}p - \frac{1}{m_v}\int_0^L w\,\rho\chi(a)\,\mathrm{d}a.\end{aligned} \tag{4.6}$$

The gradient of $\mathscr{H}$ is taken with respect to a weighted inner product. Let $Z = (x,q,w,p)$. Then the inner product is defined by

$$\langle\!\langle Z_1, Z_2\rangle\!\rangle := \int_0^L (x_1x_2 + w_1w_2)\rho\chi\,\mathrm{d}a + q_1q_2 + p_1p_2. \tag{4.7}$$

Hence the gradient of $\mathscr{H}$ is defined by

$$\frac{\mathrm{d}}{\mathrm{d}s}\mathscr{H}(Z + s\delta Z)|_{s=0} = \langle\!\langle\nabla\mathscr{H}, \delta Z\rangle\!\rangle = \int_0^L \left(\frac{\delta\mathscr{H}}{\delta x}\delta x + \frac{\delta\mathscr{H}}{\delta w}\delta w\right)\rho\chi\,\mathrm{d}a + \frac{\delta\mathscr{H}}{\delta q}\delta q + \frac{\delta\mathscr{H}}{\delta p}\delta p.$$

Associated with the system (4.6) are the boundary conditions

$$x(0,t) = 0 \quad \text{and} \quad x(L,t) = L \quad \text{for all } t, \tag{4.8}$$

and

$$w(0,t) = w(L,t) = \frac{1}{m_v}p - \frac{1}{m_v}\int_0^L w(a,t)\,\rho\chi(a)\,\mathrm{d}a \quad \text{for all } t. \tag{4.9}$$

Note that non-local term

$$\sigma(t) := \int_0^L w(a,t)\,\rho\chi(a)\,\mathrm{d}a, \tag{4.10}$$

appears both in the equations and in the boundary conditions. This non-local term will be one of the challenges in developing a numerical method. The symplectic form associated with this Hamiltonian formulation is

$$\Omega = \int_0^L \mathrm{d}w\wedge\mathrm{d}x\,\rho\chi\,\mathrm{d}a + \mathrm{d}p\wedge\mathrm{d}q. \tag{4.11}$$

https://doi.org/10.1017/S0956792510000197 Published online by Cambridge University Press

The Hamiltonian functional (4.5) is the total energy, and it is conserved along solutions.

5 Linear coupled problem

An analysis of the linear problem will be useful for determining how the natural frequencies of the fluid sloshing are modified by the coupling. The linear natural frequencies obtained by [8] in the Eulerian setting will be recovered here in the LPP setting.

5.1 Formulation of the linear problem

Let $x(a,t) = a + X(a,t)$ and $h(a,t) = h_0 + H(a,t)$, and linearize the governing equations about the trivial solution. Then $\chi(a) = h_0$ and $X(a,t)$ and $H(a,t)$ satisfy

$$X_{tt} - gh_0 X_{aa} = -q_{tt}, \tag{5.1}$$

with boundary conditions $X(0,t) = X(L,t) = 0$ and

$$H + h_0 X_a = 0, \tag{5.2}$$

and the linearized vehicle motion equation is

$$\frac{\mathrm{d}^2}{\mathrm{d}t^2}\left(\frac{m_f}{L}\int_0^L X(a,t)\,\mathrm{d}a + (m_v + m_f)q(t)\right) + vq = 0. \tag{5.3}$$

Consider solutions that are periodic in time of frequency ω:

$$X(a,t) = \widehat{X}(a)\,\sin\omega t, \quad H(a,t) = \widehat{H}(a)\,\sin\omega t, \quad q(t) = \widehat{q}\,\sin\omega t. \tag{5.4}$$

Substitution into (5.1)–(5.3) results in the coupled integro-differential system

$$\begin{aligned} &\widehat{X}_{aa} + \alpha^2\,\widehat{X} = -\alpha^2\widehat{q}, \\ &\widehat{H} + h_0\widehat{X}_a = 0, \\ &\frac{m_f}{L}\int_0^L \widehat{X}(a)\,\mathrm{d}a + (m_f + m_v)\widehat{q} = \frac{v}{\omega^2}\widehat{q}, \end{aligned} \tag{5.5}$$

where

$$\alpha = \frac{\omega}{\sqrt{gh_0}}, \tag{5.6}$$

and the boundary conditions are $\widehat{X}(0) = \widehat{X}(L) = 0$. The first two equations of (5.5) can be solved for $\widehat{q}$, $\widehat{X}$ and $\widehat{H}$,

$$\widehat{q} = -\mathsf{C}\frac{1}{\alpha h_0}\cot\frac{1}{2}\alpha L, \tag{5.7}$$

where C represents an arbitrary non-zero multiplicative constant,

$$\widehat{X}(a) = \mathsf{C}\frac{1}{\alpha h_0}\left(\cot\frac{1}{2}\alpha L(1 - \cos\alpha a) - \sin\alpha a\right), \tag{5.8}$$

https://doi.org/10.1017/S0956792510000197 Published online by Cambridge University Press

and

$$\widehat{H}(a) = \mathsf{C}\left(\cos\alpha a - \cot\tfrac{1}{2}\alpha L \sin\alpha a\right). \tag{5.9}$$

A key assumption in this derivation is

$$\sin\tfrac{1}{2}\alpha L \neq 0. \tag{5.10}$$

The implications of this singularity are discussed below. Substituting the expressions (5.7)-(5.9) into the third equation in (5.5) and using the integral

$$\int_0^L \widehat{X}(a)\,\mathrm{d}a = \mathsf{C}\frac{2}{\alpha^2 h_0}\left(\frac{1}{2}\alpha L \cot\frac{1}{2}\alpha L - 1\right),$$

gives

$$\frac{2\rho}{\alpha^2}\mathsf{C}(s\cot s - 1) - m_f\frac{\mathsf{C}}{\alpha h_0}\cot s = (m_v - v\omega^{-2})\frac{\mathsf{C}}{\alpha h_0}\cot s,$$

where

$$s = \tfrac{1}{2}\alpha L,$$

or since $\mathsf{C} \neq 0$,

$$2\frac{g}{L}m_f\alpha h_0 = (-m_v\omega^2 + v)\cot s.$$

To see that this agrees with Cooker's result recast in terms of the dimensionless parameters R and G in (3.6). Then

$$\Delta(s) = 0 \quad \text{with} \quad \Delta(s) = \frac{G}{s} - Rs - \tan s, \tag{5.11}$$

which is precisely equation (15) in [8]. Cooker shows that equation (5.11) has a countable number of positive solutions, s_j with $j = 1, 2, \ldots$. Moreover, for fixed R, G and $s > 0$ the derivative satisfies $\Delta'(s) < 0$. Hence all roots of $\Delta(s) = 0$ are simple. Given a root s_j satisfying $\Delta(s_j) = 0$, the natural frequency of the coupled system is then given by

$$\omega_j^{coupled} = \frac{2}{L}\sqrt{gh_0}\,s_j. \tag{5.12}$$

5.2 Natural frequencies

For comparison, the natural frequencies of the uncoupled problem are recorded. The fluid natural frequencies when the tank is fixed (the sloshing frequencies) are

$$\omega_j^f := 2\frac{\sqrt{gh_0}}{L}\frac{j\pi}{2}, \quad j = 1, 2, \ldots.$$

The natural frequency of the dry vessel is

$$\omega_v = \sqrt{\frac{v}{m_v}} = 2\frac{\sqrt{gh_0}}{L}\sqrt{\frac{G}{R}}.$$

https://doi.org/10.1017/S0956792510000197 Published online by Cambridge University Press

The natural frequency of the dry vessel plus fluid with the fluid treated as rigid body is

$$\omega_{fv} = \sqrt{\frac{v}{m_f + m_v}} = 2\frac{\sqrt{gh_0}}{L}\sqrt{\frac{G}{(1+R)}}.$$

Cooker shows that $\omega_1^{coupled}$ is in fact strictly less than all other natural frequencies:

$$\omega_1^{coupled} < \omega_1^f, \quad \omega_1^{coupled} < \omega_v, \quad \omega_1^{coupled} < \omega_{fv}. \tag{5.13}$$

The first inequality follows from the fact that $s_1 < \frac{1}{2}\pi$ [8]. Furthermore, $\omega_1^{coupled} \to \omega_1^f$ only in the limit $G \to \infty$. The third inequality in (5.13) is verified as follows. Use the inequality $\tan(s_1) > s_1$ (since $2s_1 < \pi$) and then

$$\frac{G}{s_1} - Rs_1 = \tan s_1 > s_1 \quad \Rightarrow \quad s_1 < \sqrt{\frac{G}{1+R}} \quad \Rightarrow \quad \omega_1^{coupled} < \omega_{fv}.$$

A similar argument confirms the second inequality in (5.13).

The singularity (5.10) can be expressed in terms of natural frequencies

$$\sin\frac{1}{2}\alpha L = 0 \quad \Rightarrow \quad \frac{1}{2}\alpha L = j\pi \quad \Rightarrow \quad \omega_j^{coupled} = 2\frac{\sqrt{gh_0}}{L}j\pi.$$

But when $s_j = j\pi$ then $\tan s_j = 0$ and so (5.11) reduces to

$$\frac{G}{j\pi} - Rj\pi = 0 \quad \text{or} \quad \frac{G}{R} = j^2\pi^2, \quad j = 1, 2, \ldots.$$

Cooker refers to this as resonance, since $G = j^2\pi^2 R$ implies that

$$\omega_j^{coupled} = \omega_v \quad \text{and} \quad \omega_v = 2\omega_j^f.$$

The main consequence of the singularity

$$\frac{G}{R} = j^2\pi^2, \quad j = 1, 2, \ldots \tag{5.14}$$

is that the class of periodic solutions (5.4) no longer exists.

5.3 Eulerian representation of linear LPP solutions

One of the surprising features of linear solutions, obtained in the LPP setting, is that they can appear highly non-linear when transformed into the Eulerian representation. Given a LPP solution, the wave height – at a particular time – in the Eulerian setting, is obtained by plotting the parametric curve

$$\{(x(a,t), h(a,t)) \ : \ t \text{ fixed and } 0 \leqslant a \leqslant L\}. \tag{5.15}$$

https://doi.org/10.1017/S0956792510000197 Published online by Cambridge University Press

Table 1. *Input data for the numerical experiments in Figures 3–21. The fluid density* $\rho = 1000\,\mathrm{kg/m^3}$, *the gravitational constant is set at* $g = 9.81\,\mathrm{m/s^2}$, *and the tank length is* $L = 0.525\,\mathrm{m}$. *In all cases the space step is* $\Delta a = 1.05 \times 10^{-4}\,\mathrm{m}$ *and time step is* $\Delta t = 10^{-4}\,\mathrm{s}$, *the number of time steps is typically* 10^6 *and the CPU time per simulation is typically 20 min*

Figures	3–5	6–8	9–11	12–14	16–18 $\dot{q}(0) = 0.4$	19–21 $q(0) = 0.15$
h_0 (m)	0.09	0.05	0.07	0.07	0.07	0.07
v (kg/s^2)	170	150.0	380.0	380.0	380.0	380.0
m_f (kg)	47.25	26.25	36.75	36.75	36.75	36.75
m_v (kg)	6.15	5.80	3.50	3.50	3.50	3.50
C (m)	0.03	0.015	0.025	0.025	–	–
ω (rad/s)	1.72078580 $= \omega_1^{coupled}$	7.51404465 $= \omega_2^{coupled}$	2.68446786 $= \omega_1^{coupled}$	18.66747146 $= \omega_3^{coupled}$	–	–
h_0/L	0.17143	0.0952	0.1333	0.1333	0.1333	0.1333
R	0.13015873	0.22095238	0.09523809	0.09523809	0.09523809	0.09523809
G	0.28079812	0.80275229 $< \pi^2 R$	1.03757099 $> \pi^2 R$	1.03757099 $> \pi^2 R$	0.93996232 $= \pi^2 R$	0.93996232 $= \pi^2 R$
$\omega_1^{coupled}$(rad/s)	1.72078580	1.98055989	2.68446786	2.68446786	2.58557248	2.58557248
ω_1^f (rad/s)	5.62271832	4.19092679	4.95877146	4.95877146	4.95877146	4.95877146
ω_v (rad/s)	5.25759222	5.08547619	10.41976144	10.41976144	9.91754292	9.91754292
ω_{fv} (rad/s)	1.78424230	2.16337402	3.07262002	3.07262002	2.92452385	2.92452385

Denote the resulting wave height in the Eulerian setting by $h(x,t)$. Then the slope of this wave height is related to the slope of the wave height in the Lagrangian setting by

$$\frac{\partial h}{\partial x} = \frac{1}{x_a}\frac{\partial h}{\partial a}.$$

Hence, when x_a is small, the slope is exaggerated in the Eulerian setting creating a non-linear appearance. Indeed, one can create highly non-linear solutions such as waves with cusp-like crests.

To see this effect consider the above linear solution in the LPP setting. Then the Eulerian wave height is obtained by plotting the parametric curve

$$\{(a + \widehat{X}(a)\sin\omega t, h_0 + \widehat{H}(a)\sin\omega t) \;:\; 0 \leqslant a \leqslant L\}, \tag{5.16}$$

for fixed values of t. In this example, the LPP wave slope is just sinusoidal, but division by x_a creates the ratio of two sinusoidal functions which is still periodic but not sinusoidal. Choosing parameter values associated with Figure 8 (parameter values listed in the second column of Table 1). The resulting sequence of parametric curves is shown in Figure 2.

The linear solutions obtained in the LPP setting and transformed to the Eulerian setting are not the same as the solutions obtained by linearizing in the Eulerian setting. The linearization in the Eulerian setting is

$$U_t + gH_x = -\ddot{q} \quad \text{and} \quad H_t + h_0 U_x = 0, \tag{5.17}$$

https://doi.org/10.1017/S0956792510000197 Published online by Cambridge University Press

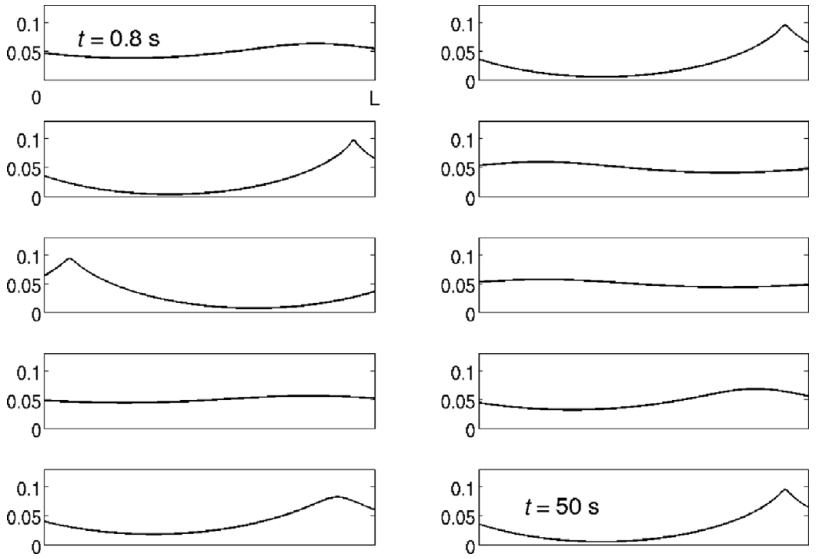


FIGURE 2. The parametric curve (5.16) plotted at a sequence of times.

with the linearized vehicle equation

$$\frac{\mathrm{d}}{\mathrm{d}t}\int_0^L \rho h_0 U \,\mathrm{d}x + (m_v + m_f)\ddot{q} + vq = 0. \tag{5.18}$$

The analogous assumption to (5.4) is

$$U(x,t) = \widehat{U}(x)\cos\omega t, \quad H(x,t) = \widehat{H}(x)\sin\omega t, \quad q(t) = \widehat{q}\sin\omega t.$$

Solving for $\widehat{H}(x)$ shows that it is

$$\widehat{H}(x) = \mathsf{C}\left(\cos\alpha x - \cot\tfrac{1}{2}\alpha L\,\sin\alpha x\right). \tag{5.19}$$

It is exactly the same as $\widehat{H}(a)$ in (5.9) with a replaced by x. Hence to capture the Eulerian linearization, $x(a,t)$ is just approximated by a.

6 Numerical algorithm – the semi-discretization

Discretize the reference space by letting

$$a_i = (i-1)\Delta a, \quad i = 1,\ldots,N+1 \quad \text{with} \quad \Delta a = \frac{L}{N},$$

and let $x_i(t) := x(a_i,t)$ and $w_i(t) := w(a_i,t)$. After choosing a discretization for the derivatives and integrals with respect to a, the governing equations can be written as a large set of ordinary differential equations. There are only two tricky points: firstly, how to discretize the right-hand side of the first equation in (4.6); secondly, how to discretize the integral term in the third and fourth equations.

https://doi.org/10.1017/S0956792510000197 Published online by Cambridge University Press

For the first difficulty, a variational discretization is used [20]: discretize the Hamiltonian functional first, and then take a variation of the discretized Hamiltonian [20]. In this case, the functional that generates the term is

$$\mathscr{F}(x) = \int_0^L -\frac{g\chi(a)}{2x_a}\,\rho\chi(a)\,\mathrm{d}a.$$

Discretize using a finite difference formula for the derivative

$$\mathscr{F}(x_1,\ldots,x_{N+1}) = \sum_{i=1}^{N} -\frac{1}{2}\frac{g\chi_i\Delta a}{(x_{i+1}-x_i)}\,\rho\chi_i\Delta a.$$

Now take a variation in $(x_1,\ldots,x_{N+1})$,

$$\frac{\mathrm{d}}{\mathrm{d}s}\bigg|_{s=0}\mathscr{F}(x_1+s\xi_1,\ldots,x_{N+1}+s\xi_{N+1}) = \sum_{i=2}^{N}\frac{g}{2\chi_i}\left(\frac{\chi_{i-1}^2\Delta a}{(x_i-x_{i-1})^2}-\frac{\chi_i^2\Delta a}{(x_{i+1}-x_i)^2}\right)\rho\xi_i\chi_i\Delta a.$$

This argument suggests that the natural semi-discretization of the first equation in (4.6) is then

$$\dot{w}_i = \frac{g\Delta a}{2\chi_i}\left(\frac{\chi_{i-1}^2}{(x_i-x_{i-1})^2}-\frac{\chi_i^2}{(x_{i+1}-x_i)^2}\right),\quad i=2,\ldots,N.$$

For the integral of w that appears in (4.6) the trapezoidal rule is used

$$\sigma_N(t) := \sum_{i=2}^{N} w_i(t)\,\rho\chi_i\Delta a + \tfrac{1}{2}\rho\,(\chi_1 w_1(t)+\chi_{N+1}w_{N+1}(t))\,\Delta a. \tag{6.1}$$

The choice of quadrature formula for σ will affect the symplecticity of the semi-discretization. In an earlier version of this manuscript, Simpson's rule was used. But, as pointed out by a referee, Simpson's rule results in a non-symplectic semi-discretization.

The full semi-discretization is then

$$\begin{aligned}
\dot{w}_i &= \frac{g\Delta a}{2\chi_i}\left(\frac{\chi_{i-1}^2}{(x_i-x_{i-1})^2}-\frac{\chi_i^2}{(x_{i+1}-x_i)^2}\right),\quad i=2,\ldots,N,\\
\dot{p} &= -vq,\\
\dot{x}_i &= w_i - \frac{1}{m_v}p + \frac{1}{m_v}\sigma_N,\quad i=2,\ldots,N,\\
\dot{q} &= \frac{1}{m_v}(p-\sigma_N),
\end{aligned} \tag{6.2}$$

with boundary conditions

$$x_1(t)=0,\quad x_{N+1}(t)=L\quad\text{and}\quad w_1(t)=w_{N+1}(t)=\frac{1}{m_v}(p(t)-\sigma_N(t)).$$

https://doi.org/10.1017/S0956792510000197 Published online by Cambridge University Press

The semi-discretization is symplectic with symplectic form

$$\Omega_N = \sum_{i=2}^{N} \mathrm{d}w_i \wedge \mathrm{d}x_i \, \rho\chi_i \Delta a + \mathrm{d}p \wedge \mathrm{d}q.$$

The proof of symplecticity is straightforward but lengthy and is therefore given in the technical report [3]. The semi-discretization is Hamiltonian and the Hamiltonian functional is a discretization of the energy,

$$\begin{aligned}\mathscr{H}_N = \frac{1}{2}\rho \sum_{i=2}^{N} \chi_i w_i^2 \Delta a + \frac{1}{4}\rho\left(\chi_1 w_1^2 + \chi_{N+1} w_{N+1}^2\right)\Delta a \\ + \frac{1}{2}\rho g \sum_{i=1}^{N} \frac{\chi_i^2 \Delta a^2}{(x_{i+1} - x_i)} + \frac{1}{2m_v}(p - \sigma_N)^2 + \frac{1}{2} v q^2.\end{aligned} \tag{6.3}$$

This energy is conserved along orbits of the semi-discretization. This latter property can be verified by introducing an appropriate inner product for the semi-discretization and using the fact that $\mathscr{H}_N$ is the Hamiltonian function that generates the equations (6.2).

7 Numerical algorithm – time discretization using Störmer–Verlet

The semi-discretization (6.2) is of the form

$$\begin{aligned}\dot{\mathbf{p}} &= g(\mathbf{q}), \\ \dot{\mathbf{q}} &= f(\mathbf{p}),\end{aligned}$$

where

$$\mathbf{p} = (p, w_2, \ldots, w_N) \quad \text{and} \quad \mathbf{q} = (q, x_2, \ldots, x_N).$$

The precise form of $f(\cdot)$ and $g(\cdot)$ can be deduced from (6.2) but will not be needed. The important point here is the fact that the right-hand side of the $\dot{\mathbf{p}}$ equation depends only on $\mathbf{q}$ and the right-hand side of the $\dot{\mathbf{q}}$ equation depends only on $\mathbf{p}$. There are appealing numerical methods for equations of this form: split-step methods, or partitioned Runge–Kutta methods (e.g. Section 2.5 of [18]).

7.1 Time integration using the Störmer–Verlet algorithm

One of the simplest of the class of split-step methods is the discretization

$$\begin{aligned}\mathbf{p}^{n+\frac{1}{2}} &= \mathbf{p}^n + \tfrac{1}{2}\Delta t \, g\left(\mathbf{q}^n\right), \\ \mathbf{q}^{n+1} &= \mathbf{q}^n + \Delta t \, f\left(\mathbf{p}^{n+\frac{1}{2}}\right), \\ \mathbf{p}^{n+1} &= \mathbf{p}^{n+\frac{1}{2}} + \tfrac{1}{2}\Delta t \, g(\mathbf{q}^{n+1}).\end{aligned} \tag{7.1}$$

This scheme is explicit, and has second-order accuracy in time. If in addition the equations are Hamiltonian as in (6.2) then this scheme is called the *Störmer–Verlet* algorithm and it

https://doi.org/10.1017/S0956792510000197 Published online by Cambridge University Press

has additional properties [13, 18]. It is symplectic, and has excellent energy conservation over long-time intervals.

Applying (7.1) to the semi-discretization (6.2) gives the following equations for each time step $n \mapsto n+1$

$$\begin{aligned}
p^{n+\frac{1}{2}} &= p^n - \frac{\Delta t}{2} v q^n,\\
w_i^{n+\frac{1}{2}} &= w_i^n + \frac{g\Delta t \Delta a}{4\chi_i}\left(\frac{\chi_{i-1}^2}{\left(x_i^n - x_{i-1}^n\right)^2} - \frac{\chi_i^2}{\left(x_{i+1}^n - x_i^n\right)^2}\right), \quad i = 2,\ldots,N,\\
x_i^{n+1} &= x_i^n + \Delta t w_i^{n+\frac{1}{2}} - \frac{\Delta t}{m_v} p^{n+\frac{1}{2}} + \frac{\Delta t}{m_v}\sigma_N^{n+\frac{1}{2}}, \quad i = 2,\ldots,N,\\
q^{n+1} &= q^n + \frac{\Delta t}{m_v} p^{n+\frac{1}{2}} - \frac{\Delta t}{m_v}\sigma_N^{n+\frac{1}{2}},\\
p^{n+1} &= p^{n+\frac{1}{2}} - \frac{\Delta t}{2} v q^{n+1},\\
w_i^{n+1} &= w_i^{n+\frac{1}{2}} + \frac{g\Delta t \Delta a}{4\chi_i}\left(\frac{\chi_{i-1}^2}{\left(x_i^{n+1} - x_{i-1}^{n+1}\right)^2} - \frac{\chi_i^2}{\left(x_{i+1}^{n+1} - x_i^{n+1}\right)^2}\right), \quad i = 2,\ldots,N,
\end{aligned} \tag{7.2}$$

where

$$w_i^n = w(a_i, t_n), \quad x_i^n = x(a_i, t_n), \quad p^n = p(t_n), \quad q^n = q(t_n), \quad t_n = n\Delta t,$$

and the boundary conditions are

$$x_1^{n+1} = 0 \quad \text{and} \quad x_{N+1}^{n+1} = L, \tag{7.3}$$

and

$$w_1^{n+\frac{1}{2}} = w_{N+1}^{n+\frac{1}{2}} = \frac{1}{m_v}\left(p^{n+\frac{1}{2}} - \sigma_N^{n+\frac{1}{2}}\right). \tag{7.4}$$

Comparing (7.4) with the definition of σ_N shows that $w_1^{n+\frac{1}{2}}$ also appears in $\sigma_N^{n+\frac{1}{2}}$. However, combining these two equations gives an explicit expression for $\sigma_N^{n+\frac{1}{2}}$,

$$\sigma_N^{n+\frac{1}{2}} = \frac{1}{1+\gamma}\sum_{i=2}^{N} w_i^{n+\frac{1}{2}} \rho\chi_i \Delta a + \frac{\gamma}{1+\gamma} p^{n+\frac{1}{2}}, \tag{7.5}$$

where γ is independent of time

$$\gamma = \frac{\rho}{m_v}\left(\frac{\chi_1 + \chi_{N+1}}{2}\right)\Delta a.$$

Now (7.4) is implemented with the revised definition of $\sigma_N^{n+\frac{1}{2}}$ in (7.5).

The Störmer-Verlet discretization (7.2) is symplectic. The symplectic form of the discretization is

$$\Omega_N^n = \sum_{i=2}^{N} \mathrm{d}w_i^n \wedge \mathrm{d}x_i^n \, \rho\chi_i \Delta a + \mathrm{d}p^n \wedge \mathrm{d}q^n.$$

https://doi.org/10.1017/S0956792510000197 Published online by Cambridge University Press

This symplectic form satisfies $\Omega_N^{n+1} = \Omega_N^n$ for all n. The proof of this identity is an essential but lengthy digression for the paper, and therefore it is given in the freely available technical report [3].

7.2 Energy conservation

The energy (1.3) of the coupled system, transformed to the LPP setting is

$$\mathscr{E}(t) = \int_0^L \left(\frac{1}{2}(U + \dot{q})^2 + \frac{1}{2} g \frac{\chi}{x_a} \right) \rho \chi(a)\, \mathrm{d}a + \frac{1}{2} m_v \dot{q}^2 + \frac{1}{2} v q^2. \tag{7.6}$$

This energy is conserved by the coupled equations (1.4)–(4.2). Indeed when transformed to canonical coordinates (q, x, p, w) it is the Hamiltonian function (4.5).

The semi-discretization (6.2) also conserves an exact energy $\mathscr{H}_N$ defined in (6.3). The energy $\mathscr{H}_N$ is an approximation to the exact energy, but it is exactly conserved by the semi-discretization.

On the other hand the discretization (7.2) does not conserve any energy exactly. However, the best approximation to that energy is $\mathscr{H}_N$.

One of the great advantages of symplectic algorithms is that they generally have very good energy conservation. For Hamiltonian ODEs, it has been proved that the error remains small for extraordinarily long times. A precise statement can be found in Section 5.2.2 in [18]. For Störmer–Verlet the precise statement is proved in [13]. On the other hand, for *semi-discretizations* the theory is not clear; see [23]) for recent work in conservation of first integrals for semi-discretizations. However, our numerical experiments so show excellent energy conservation. For over one million time steps the energy error remains bounded with only very small drift.

8 Numerical simulations – linear system

The first simulations are of the linearized coupled equations, derived in Section 5. For the simulations, the Hamiltonian formulation is required and this is derived below. The linear simulations provide an opportunity to test the algorithm by comparing to the exact solution for time-periodic solutions, and to determine the nature of the solutions near resonance.

8.1 Linear simulations – formulation

The linearized system is

$$\begin{aligned} -\dot{w} &= -g h_0 X_{aa}, \\ -\dot{p} &= v q, \\ \dot{X} &= w - \frac{1}{m_v} p + \frac{1}{LR} \int_0^L w \, \mathrm{d}a, \\ \dot{q} &= \frac{1}{m_v} p - \frac{1}{LR} \int_0^L w \, \mathrm{d}a. \end{aligned} \tag{8.1}$$

https://doi.org/10.1017/S0956792510000197 Published online by Cambridge University Press

This system is also Hamiltonian with functional

$$\begin{aligned}\mathscr{H}(X,q,w,p) = \frac{1}{2}\rho h_0 \int_0^L w^2 \,\mathrm{d}a - \frac{\rho h_0}{m_v} p \int_0^L w \,\mathrm{d}a + \frac{1}{2}\frac{1}{m_v} p^2 \\ + \frac{1}{2}\frac{\rho^2 h_0^2}{m_v}\left(\int_0^L w \,\mathrm{d}a\right)^2 + \frac{1}{2} v q^2 + \frac{1}{2}\rho g h_0^2 \int_0^L X_a^2 \,\mathrm{d}a.\end{aligned} \tag{8.2}$$

The gradient of this Hamiltonian function gives the right-hand side of (8.1), when the following weighted inner product is used

$$\langle\langle Z_1, Z_2 \rangle\rangle := \int_0^L (x_1 x_2 + w_1 w_2)\rho h_0 \,\mathrm{d}a + q_1 q_2 + p_1 p_2. \tag{8.3}$$

The system (8.1) is discretized using a centred finite-difference formula for X_{aa}, the trapezoidal rule for the integral of w and Störmer–Verlet for time integration, as in Section 7. The boundary conditions are the same as (7.3) and (7.4).

8.2 Linear simulations – away from resonance

The first simulation is a comparison with the exact oscillatory solution of Section 5. For this simulation, take initial data

$$X(a,0) = 0 \quad \text{and} \quad q(0) = 0,$$

and the momenta,

$$w(a,0) = \omega\widehat{q} + \omega\widehat{X}(a) \quad \text{and} \quad p(0) = (m_v + m_f)\omega\widehat{q} + \omega\frac{m_f}{L}\int_0^L \widehat{X}(a)\,\mathrm{d}a, \tag{8.4}$$

where $\widehat{q}$ and $\widehat{X}$ are defined in (5.7) and (5.8). Once the parameters are fixed, the frequency ω is obtained by solving $\Delta(s) = 0$, defined in (5.11), using Newton's method, and then substituting the value of s into (5.12). The chosen values of the parameters are listed in Table 1. The values are guided by the experiments in [8]. The spring stiffness in [8] is determined by the restoring force due to gravity in the suspension cables

$$v = \frac{g}{\ell}(m_v + m_f),$$

where ℓ is the length of the suspension cable. Based on the range of values for ℓ, m_v and m_f in the experiments, the range of v is

$$10.3 < v < 746.9 \quad (\mathrm{kg/s^2}).$$

Moreover, the range of R and G in the experiments in [8] is

$$0.075 < R < 3.935 \quad \text{and} \quad 0.32 < G < 73.5.$$

Take the spring stiffness to be $v = 170\,\mathrm{kg/s^2}$ and take $\omega = \omega_1^{coupled}$. The other parameter values are in the first column of Table 1. Figure 3 shows the numerical and exact solutions

https://doi.org/10.1017/S0956792510000197 Published online by Cambridge University Press

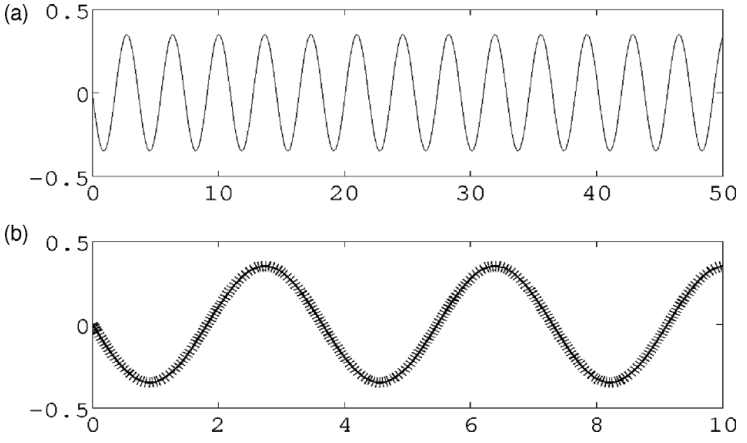


FIGURE 3. (a) Computed horizontal tank position $q(t)$ (in metres) versus time (in seconds). q is the absolute position of the vehicle as shown in Figure 1. (b) Comparison of numerical and exact solution for the first 10 s.

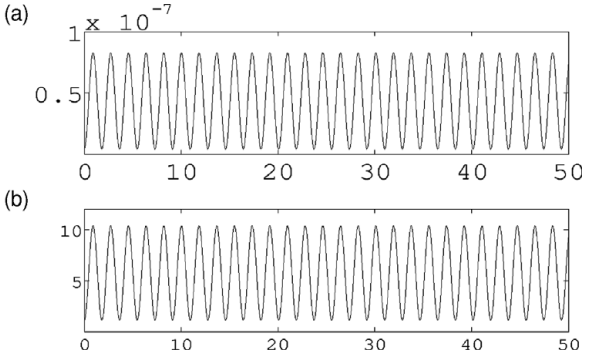


FIGURE 4. (a) Energy error associated with Figure 3. The horizontal axis is time and the vertical axis is $\mathscr{H}_N^n - \mathscr{H}_N^0$, which is the time discretization of $\mathscr{H}_N$ in (6.3). (b) The discretized energy of the vessel defined in (8.5) for $.5 \times 10^6$ time steps.

for the vehicle position, and in Figure 4 the energy error is shown. In Figure 4(b) the energy of the vehicle, E_v, is shown. The vehicle energy is defined by

$$E_v := \tfrac{1}{2} m_v \dot{q}^2 + \tfrac{1}{2} v q^2. \tag{8.5}$$

In Hamiltonian coordinates the vehicle energy is

$$E_v := \frac{1}{2m_v}(p - v)^2 + \frac{1}{2} v q^2.$$

The energy is very well conserved and follows the pattern predicted by the theory [18]. There is a shift in the mean value of the energy and the oscillations remain bounded, and appear to be close to order Δt^2. There is no noticeable drift in the energy over the $.5 \times 10^6$ time steps. The energy of the vehicle remains bounded for all time, so there does

https://doi.org/10.1017/S0956792510000197 Published online by Cambridge University Press

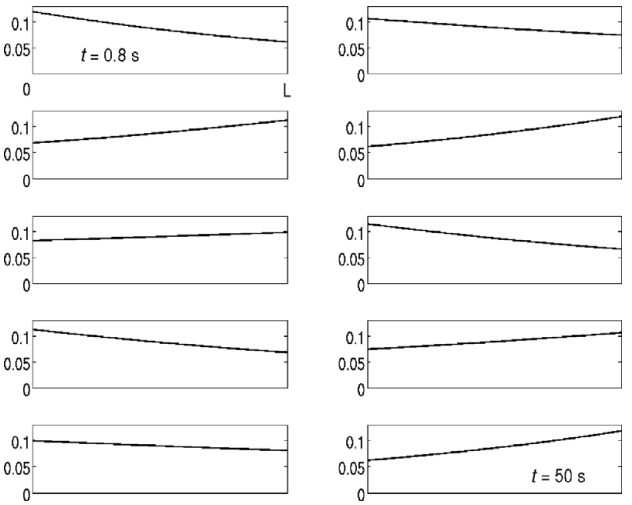


FIGURE 5. Snapshots of Eulerian wave profile associated with Figure 3. Plotted using the parametric representation of $x(a,t)$ and $h(a,t)$ for $0 \leqslant a \leqslant L$ as in (5.15).

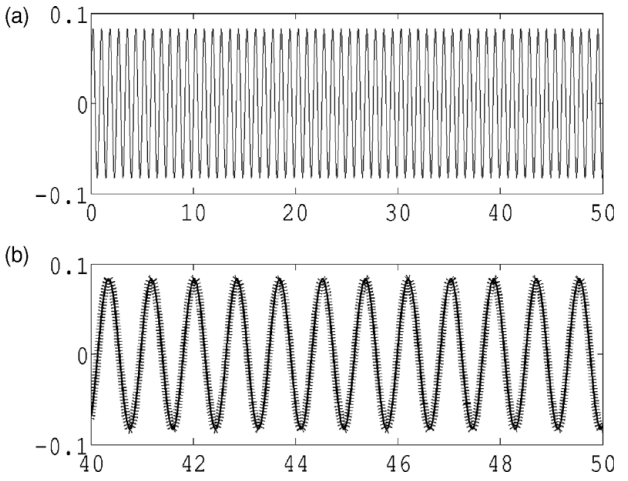


FIGURE 6. (a) Computed horizontal tank position $q(t)$ (in metres) versus time (in seconds). q is the absolute position of the vehicle as shown in Figure 1. (b) Comparison of numerical and exact solution, when $\omega = \omega_2^{coupled}$ and $G < \pi^2 R$.

not appear to be any error in the partition of energy between the vehicle and the fluid. Snapshots of the Eulerian wave profile for this case are shown in Figure 5.

Now consider the case where $\omega = \omega_2^{coupled}$, $\nu = 150\,\mathrm{kg/s^2}$ and $G < \pi^2 R$. The line $G = \pi^2 R$ is the $j = 1$ resonance curve in (5.14). The input data is tabulated in the second column of Table 1. The numerical and exact solutions are shown in Figure 6, energy error in Figure 7 and snapshots in the Eulerian representation are shown in Figure 8. The computed wave height in Figure 8 is to be compared with the exact solution in Figure 2, corresponding to the same parameter values. The agreement is excellent, with insignificant phase error.

https://doi.org/10.1017/S0956792510000197 Published online by Cambridge University Press

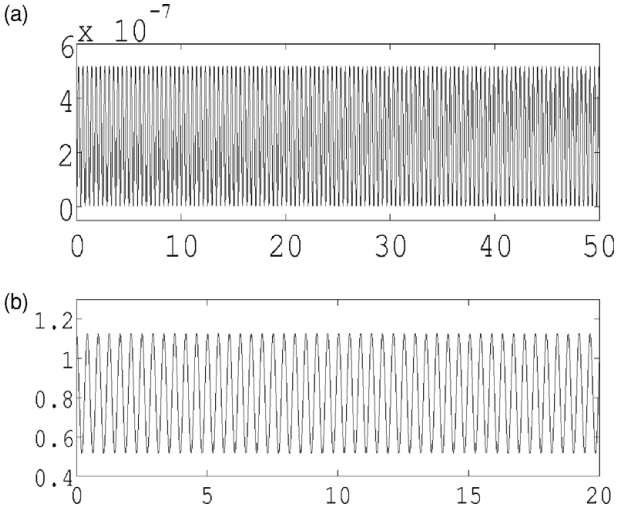


FIGURE 7. (a) Energy error associated with Figure 6. The horizontal axis is time and the vertical axis is $\mathscr{H}_N^n - \mathscr{H}_N^0$, which is the time discretization of $\mathscr{H}_N$ in (6.3). (b) The discretized energy of the vessel defined in (8.5) for the first 20 s.

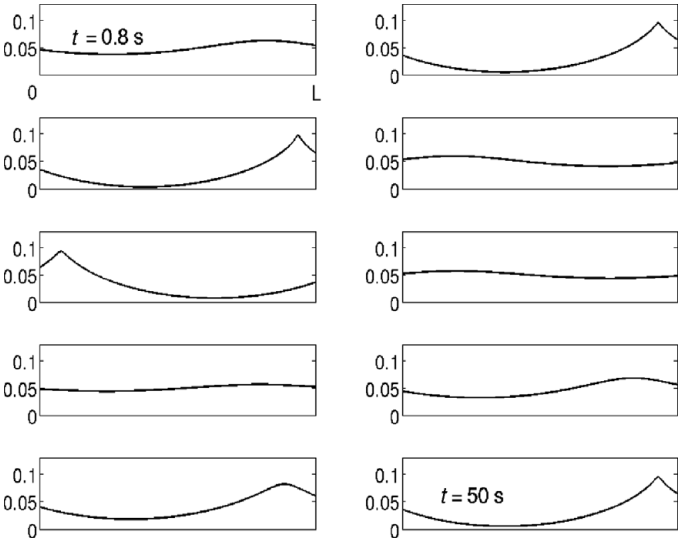


FIGURE 8. Snapshots of Eulerian wave profile associated with Figure 6. Plotted using the parametric representation of $x(a,t)$ and $h(a,t)$ for $0 \leqslant a \leqslant L$ as in (5.15).

Now consider the case where $\omega = \omega_1^{coupled}$, $v = 380\,\mathrm{kg/s^2}$ and $G > \pi^2 R$. With the input data tabulated in the third column of Table 1, the numerical and exact solutions are shown in Figure 9, energy error in Figure 10 and the snapshots in the Eulerian representation in Figure 11.

Consider the same parameter values as Figure 9 but take the frequency equal to the third natural frequency of the coupled problem, with $G > \pi^2 R$. With the input data tabulated in

https://doi.org/10.1017/S0956792510000197 Published online by Cambridge University Press

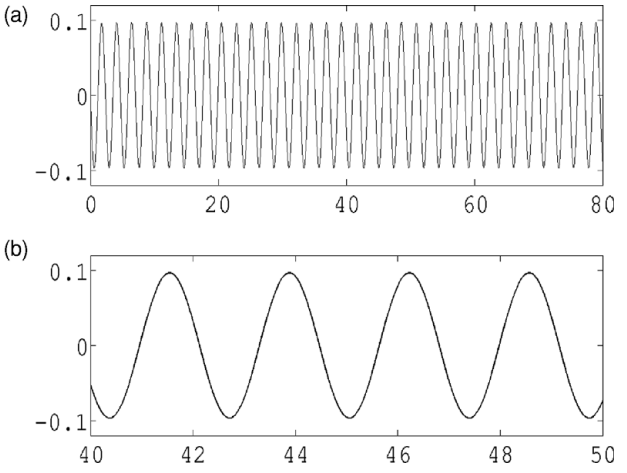


FIGURE 9. (a) Computed vehicle position versus time. (b) Expansion of the time sub-interval $40 \leqslant t \leqslant 50$. Parameters correspond to $\omega = \omega_1^{coupled}$ and $G > \pi^2 R$.

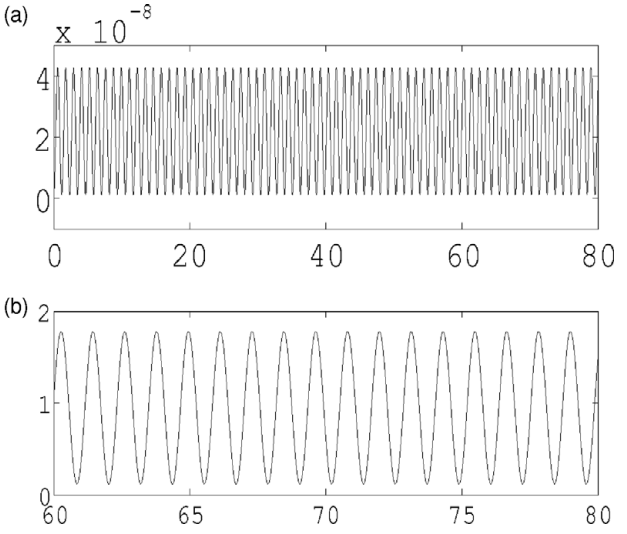


FIGURE 10. (a) Energy error associated with Figure 9. (b) Energy of the vessel versus time.

the fourth column of Table 1, the numerical and exact solutions are shown in Figure 12, energy error in Figure 13, and snapshots of the Eulerian wave profile in Figure 14. In Figure 14 a multi-peak wave shows up due to the fact that a higher mode is simulated.

To contrast the Eulerian representation of the free surface in Figure 14, obtained by transforming the Lagrangian description, the linearized Eulerian profile is shown in Figure 15. As noted in Section 5.3, the linearized Eulerian representation is just the Lagrangian representation with a replaced by x.

https://doi.org/10.1017/S0956792510000197 Published online by Cambridge University Press

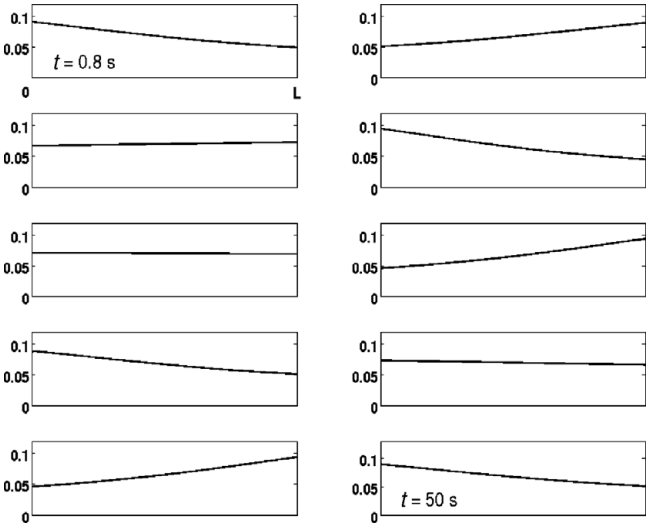


FIGURE 11. Snapshots of Eulerian wave profile associated with Figure 9.

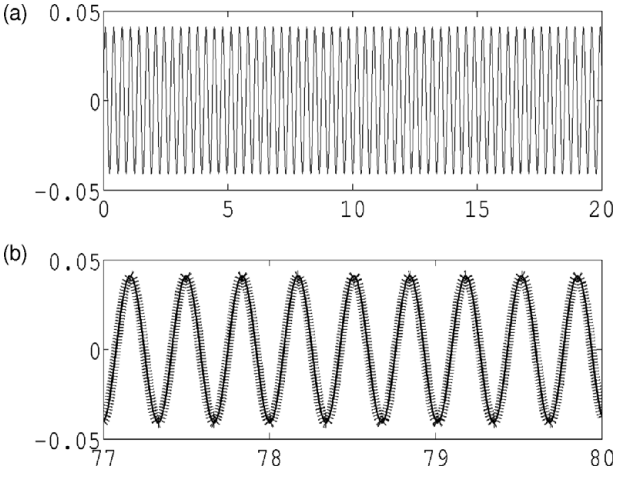


FIGURE 12. (a) Computed vehicle position versus time. (b) Numerical and exact solutions for the sub-interval $77 < t < 80$ s.

8.3 Simulations near resonance

Consider the case of of 'resonance', when $G = j^2\pi^2 R$. The most interesting case is $j = 1$. In this case ω_v is equal to $\omega_1^{coupled}$ and $\omega_v = 2\omega_1^f$. However the line $G = j^2\pi^2 R$ is not a resonance in the usual sense since ω_v and ω_1^f are not natural frequencies of the coupled problem. Nevertheless, this line in parameter space is of interest since the harmonic solution of Section 5 is no longer valid.

https://doi.org/10.1017/S0956792510000197 Published online by Cambridge University Press

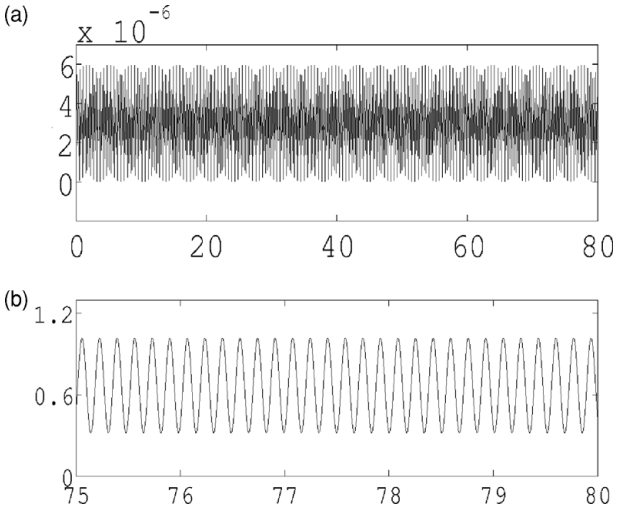


FIGURE 13. (a) Energy error associated with Figure 12. (b) Energy of the vessel versus time for the interval $75 < t < 80$ s.

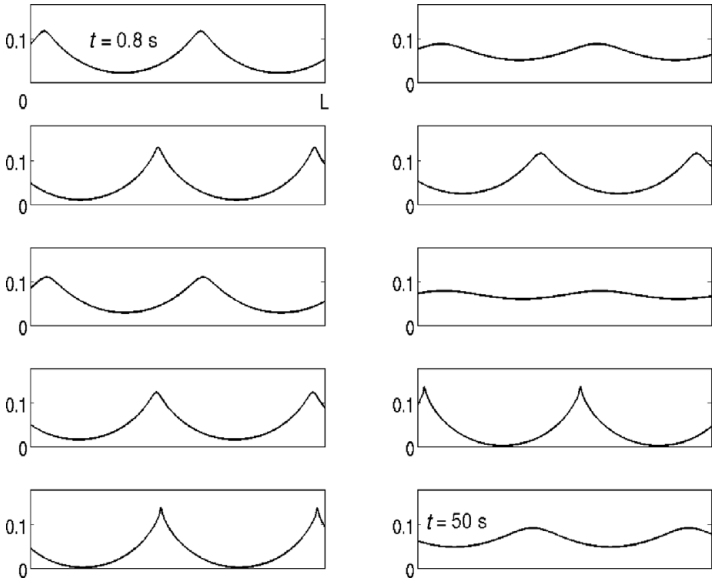


FIGURE 14. Snapshots of Eulerian wave profile associated with Figure 12.

In the resonance case the initial conditions (8.4) are no longer valid, and so the following initial conditions are used

$$h(a,0) = h_0, \quad X(a,0) = 0, \quad q(0) = 0,$$
$$w(a,0) = \dot{q}(0), \quad p(0) = \left(m_v + m_f\right)\dot{q}(0),$$

with $\dot{q}(0) \neq 0$ specified.

https://doi.org/10.1017/S0956792510000197 Published online by Cambridge University Press

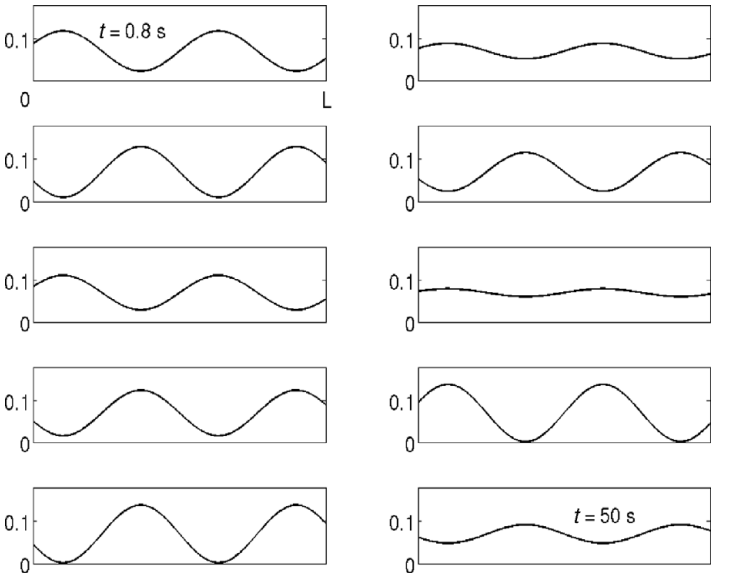


FIGURE 15. Snapshots of linearized Eulerian wave profile associated with Figure 12: a plot of a versus $h(a,t)$ for $0 \leqslant a \leqslant L$.

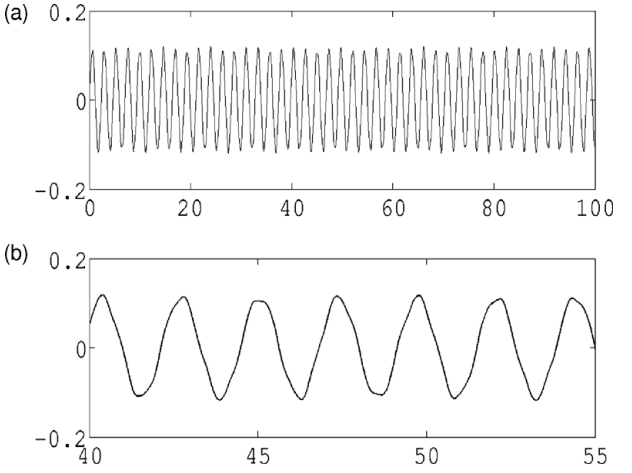


FIGURE 16. Linear simulation at resonance: (a) computed vessel position for 10^6 time steps. (b) Expansion of the time sub-interval $40 \leqslant t \leqslant 55$ s.

Setting $\dot{q}(0) = 0.40$, and with the other parameter values tabulated in Table 1, the results of numerical test for vehicle horizontal motion and energy error at different values of time are shown in Figures 16 and 17. Snapshots of the Eulerian wave profile are shown in Figure 18. Although the solution looks periodic there are clearly higher harmonics in the solution.

Now consider the case where the initial position of the vehicle, $q(0)$, is non-zero and the initial velocity, $\dot{q}(0)$, is zero. The initial fluid configuration is taken to be quiescent.

https://doi.org/10.1017/S0956792510000197 Published online by Cambridge University Press

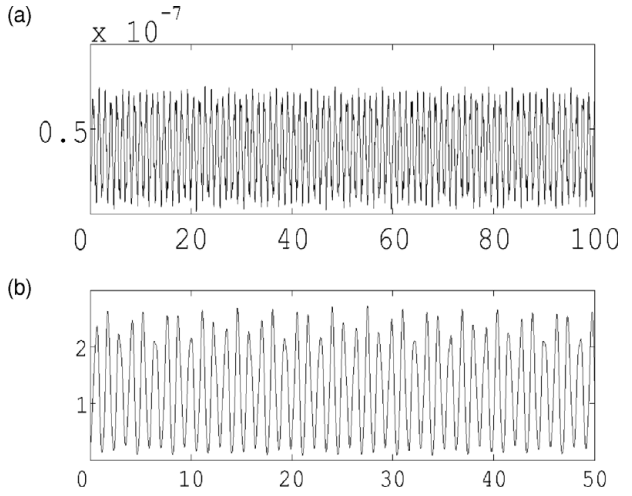


FIGURE 17. (a) Energy error associated with Figure 16. (b) Energy of the vessel versus time.

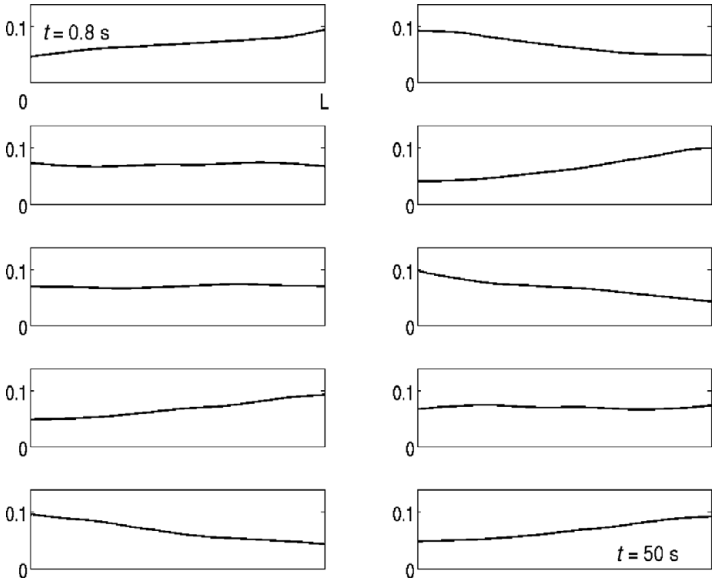


FIGURE 18. Snapshots of Eulerian wave profile associated with Figure 16.

The complete set of initial conditions is

$$h(a,0) = h_0, \quad X(a,0) = 0, \quad q(0) \neq 0,$$
$$w(a,0) = 0, \quad p(0) = 0, \quad \dot{q}(0) = 0.$$

Set $q(0) = 0.15$, with the other parameter values as tabulated in Table 1. The results of the numerical test for vehicle horizontal motion and energy error at different values of time are shown in Figures 19 and 20. Snapshots of the Eulerian wave profile are shown in

https://doi.org/10.1017/S0956792510000197 Published online by Cambridge University Press

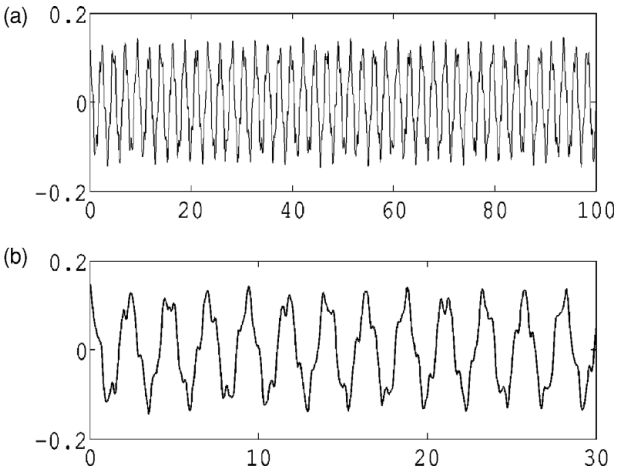


FIGURE 19. Linear simulation at resonance: (a) Vessel position plotted versus time for 10^6 time steps. (b) Solution at early time: $0 \leqslant t \leqslant 30$ s.

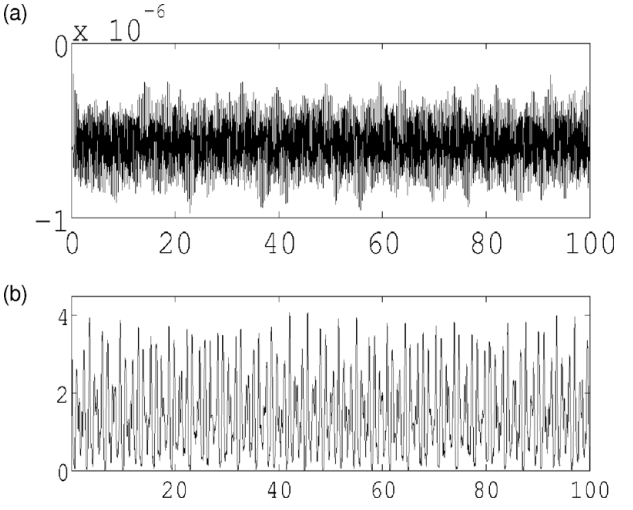


FIGURE 20. (a) Energy error associated with Figure 19. (b) Energy of vessel versus time for 10^6 time steps.

Figure 21. This simulation shows that distinctly non-harmonic behaviour of the solution near resonance.

9 Numerical simulations – non-linear system

Now consider simulation of the full non-linear discretization (7.2). For the initial conditions the fluid is taken to be quiescent and non-zero initial conditions are applied to the vehicle.

For the first simulation, take $v = 130\,\mathrm{kg/s^2}$, and set the initial velocity of the vehicle at $\dot{q}(0) = 0.1\,\mathrm{m/s}$. The other parameter values are listed in the first column of Table 2. The

https://doi.org/10.1017/S0956792510000197 Published online by Cambridge University Press

Table 2. *Input data for the numerical experiments in Figures 22–28. The fluid density* $\rho = 1000\,\mathrm{kg/m^3}$, *the gravitational constant is set at* $g = 9.81\,\mathrm{m/s^2}$, *and the tank length is* $L = 0.525\,\mathrm{m}$. *The space step and time step in all cases are* $\Delta a = 1.05\times10^{-4}\,\mathrm{m}$ *and* $\Delta t = 10^{-4}\,s$, *the number of time steps is* 10^6 *and the CPU time per simulation is typically about 20 min*

Figure	22 and 24	25 and 27	28
h_0 (m)	0.08	0.06	0.05
v (kg/s^2)	130.0	35.0	0.0
m_f (kg)	42.0	31.50	26.25
m_v (kg)	8.40	11.025	13.125
$\dot{q}(0)$ (m/s)	0.10	0.0	0.01
$q(0)$ (m)	0.0	0.05	0.0
h_0/L	0.1524	0.1143	0.0952
R	0.20	0.35	0.50
G	0.27176509	0.13007560	0.0
$\omega_1^{coupled}$ (rad/s)	1.55655499	0.89646318	–
ω_1^f (rad/s)	5.30114967	4.59093028	4.19092679
ω_v (rad/s)	3.93397893	1.78174162	0.0
ω_{fv} (rad/s)	1.60604018	0.90721842	0.0

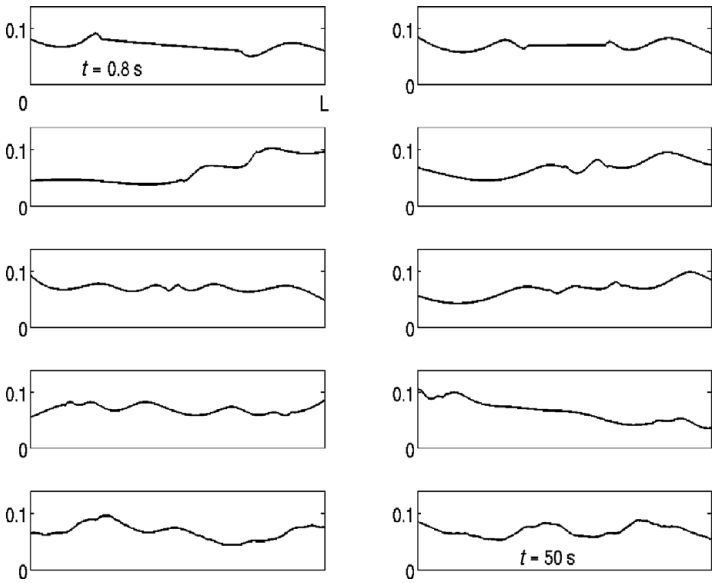


FIGURE 21. Snapshots of Eulerian wave profile associated with Figure 19.

complete set of initial conditions is

$$h(a,0) = h_0, \quad x(a,0) = a, \quad q(0) = 0,$$
$$\dot{q}(0) = 0.1, \quad w(a,0) = \dot{q}(0), \quad p(0) = (m_v + m_f)\dot{q}(0).$$

https://doi.org/10.1017/S0956792510000197 Published online by Cambridge University Press

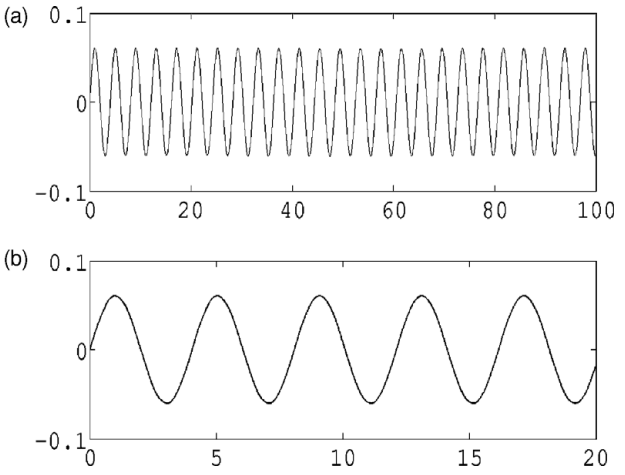


FIGURE 22. Simulation of the non-linear coupled system: (a) computed vehicle horizontal motion versus time for 10^6 time steps. (b) Vehicle position for for first 20 s.

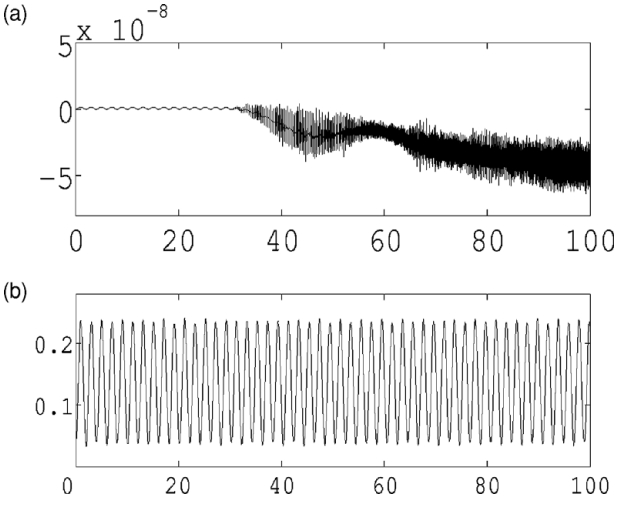


FIGURE 23. (a) Energy error versus time associated with Figure 22. (b) Energy of the vessel versus time.

The computed vehicle horizontal motion and energy error are shown in Figures 22 and 23. Snapshots of Eulerian wave profile are shown in Figure 24. Although the energy conservation is still excellent, with an error close to order Δt^2, the non-linearity now appears to be inducing a slow drift with time. But even over 10^6 time steps this drift is small.

For the second non-linear simulation, take $v = 35\,\mathrm{kg/s^2}$ and set the initial position of the vehicle to be non-zero. Other parameter values are listed in the second column of Table 2. The complete set of initial conditions is

$$h(a,0) = h_0, \quad x(a,0) = a, \quad q(0) = 0.05,$$
$$\dot{q}(0) = 0, \quad w(a,0) = 0, \quad p(0) = 0.$$

https://doi.org/10.1017/S0956792510000197 Published online by Cambridge University Press

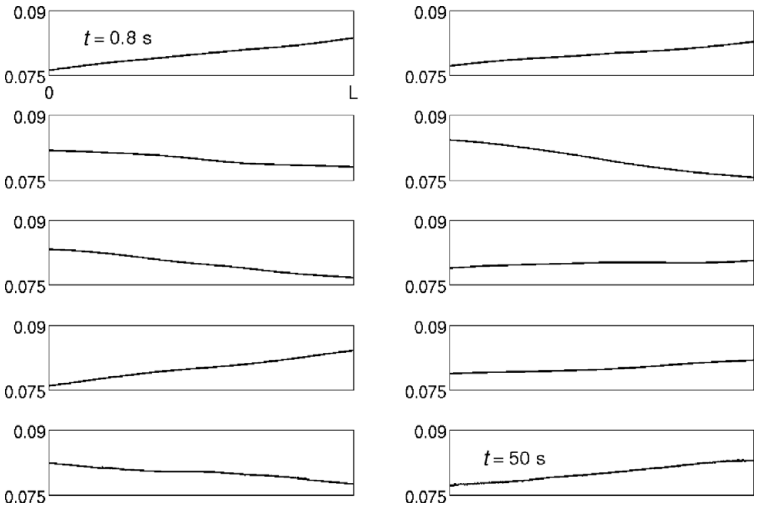


FIGURE 24. Snapshots of Eulerian wave profile associated with Figure 22.

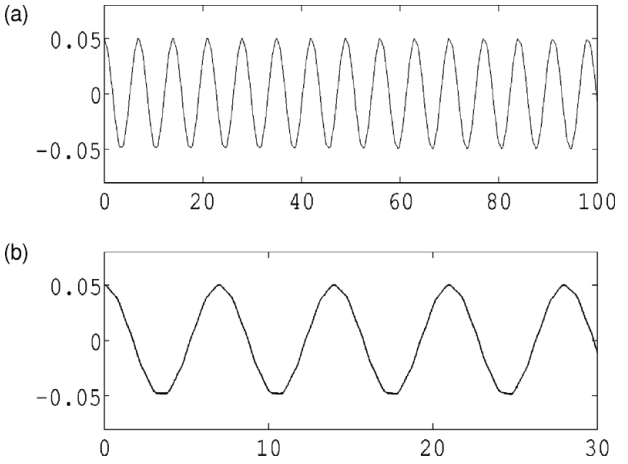


FIGURE 25. Simulation of the non-linear coupled system: (a) computed vehicle horizontal motion versus time for 10^6 time steps when $q(0) = 0.05$ and $\dot{q}(0) = 0$. (b) Numerical solution for the first 30 s.

The computed vehicle horizontal motion and energy error are shown in Figures 25 and 26. Snapshots of Eulerian wave profile are shown in Figure 27.

The third numerical experiment is to give the free surface an initial displacement, with the fluid quiescent, and determine the motion of the vehicle when the spring force is neglected. The initial free surface position is

$$h(a,0) = h_0 + \left(\frac{L}{2} - a\right)\tan\theta_0. \tag{9.1}$$

https://doi.org/10.1017/S0956792510000197 Published online by Cambridge University Press

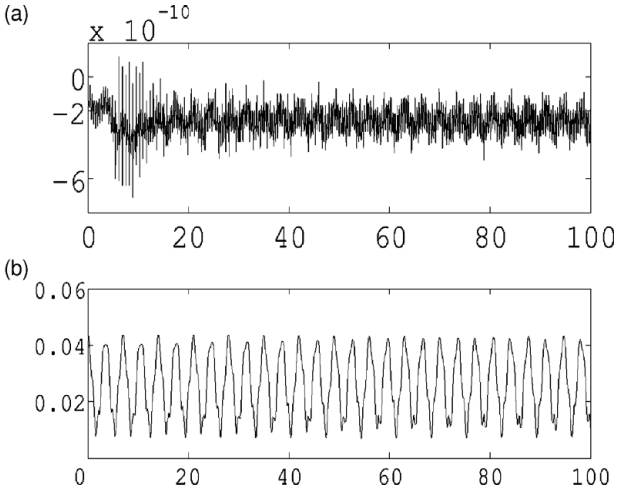


FIGURE 26. (a) Energy error associated with Figure 25. (b) Energy of the vessel versus time.

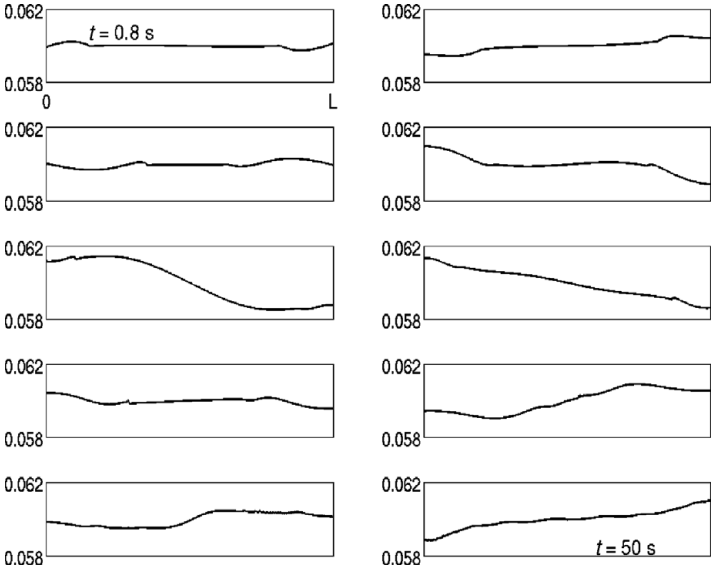


FIGURE 27. Snapshots of Eulerian wave profile associated with Figure 25.

In this case the function $\chi(a)$ is

$$\chi(a) := hx_a|_{t=0} = h(a,0) = h_0 + \left(\frac{L}{2} - a\right)\tan\theta_0.$$

With the input data tabulated in the last column of Table 2, the numerical solution for $q(t)$ and the energy error are shown in Figures 28 and 29.

https://doi.org/10.1017/S0956792510000197 Published online by Cambridge University Press

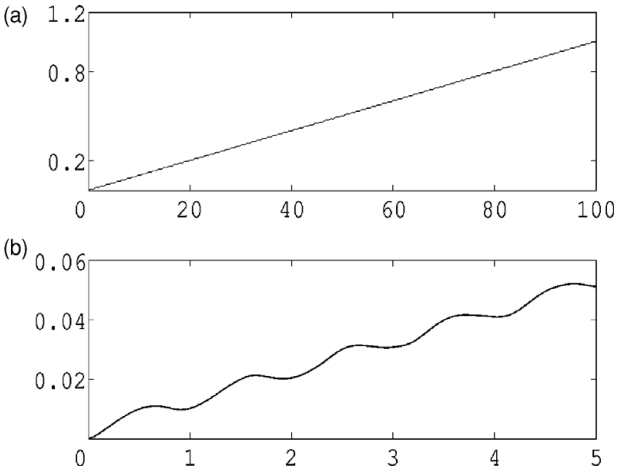


FIGURE 28. Simulation of the non-linear coupled system when $v = 0$. The initial surface profile is (9.1) with $\theta_0 = -0.5^{\circ}$. (a) Numerically computed vehicle position versus time for 10^6 time steps. (b) Numerical solution for the first 5 s.

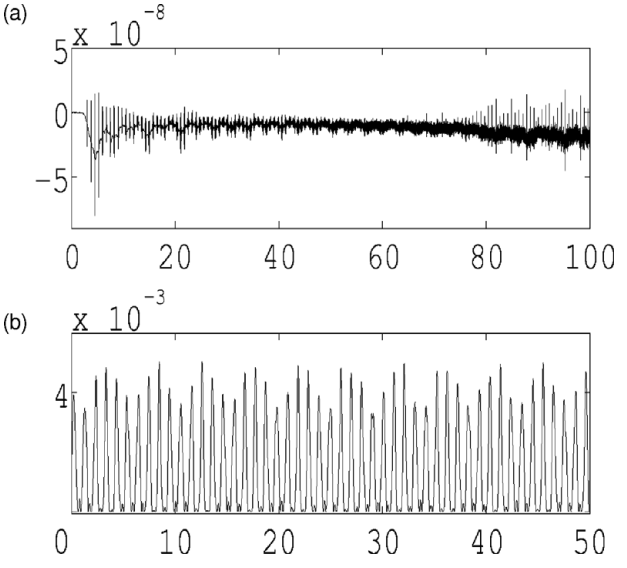


FIGURE 29. (a) Energy error associated with Figure 28. (b) Energy of the vessel versus time.

There is a slow drift of the vehicle due to the lack of the horizontal restoring force. When $v = 0$ the equation for $q(t)$ can be integrated (see Appendix C),

$$\int_0^L x(a,t)\rho\chi(a)\,\mathrm{d}a + (m_v + m_f)q(t) = \mathsf{c}_1 t + \mathsf{c}_0.$$

https://doi.org/10.1017/S0956792510000197 Published online by Cambridge University Press

Substituting for the initial data gives

$$q(t) = \dot{q}(0)\, t - \frac{1}{L}\int_0^L [x(a,t) - a]\frac{\chi(a)}{h_0}\, \mathrm{d}a. \tag{9.2}$$

The first term gives a uniform drift. With $\dot{q}(0) = 0.01$ m/s the drift should amount to about 1 m after 100 s and this is observed in the upper graph in Figure 28. The second term in (9.2) gives a small 'wobble' to the vehicle motion due to the oscillation of the fluid centre of mass. By zooming in on the graph of $q(t)$ versus t for short times, this oscillation can be seen and is shown in part (b) of Figure 28. The energy error is of order 10^{-8} for all time. When $v = 0$ the first coupled natural frequency, $\omega_1^{coupled}$, does not exist since $G = 0$ and so $\Delta(s) = -Rs - \tan s$ which has no solutions in the interval $0 < s < \frac{1}{2}\pi$.

10 Concluding remarks

The coupled problem of shallow-water sloshing and vehicle dynamics based on Cooker's experiment has been studied. The advantage of Cooker's model is that it is about the simplest configuration where one can study the coupled dynamics. The emphasis in this paper has been development of a numerical method which accurately represents the dynamics and the energy budget.

Although the coupling is non-linear, the vehicle model is linear (linear spring). A direction of great interest is to study the coupled problem with a fully non-linear vehicle motion. Two ways that non-linearity can enter are by using a non-linear spring, or by using a non-linear restoring force. The latter case arises when a non-linear model for Cooker's experiment is constructed because there the restoring force is due to gravity. Progress towards this aim is reported in the technical report [2]. This report derives the general coupled equations for sloshing that is dynamically coupled to a vehicle undergoing horizontal translation, vertical translation and rotation in the plane.

One of the main results of this paper is the adaption of numerical scheme which respects the energy budget. It is of interest to preserve the total energy in the numerical scheme, but also to maintain the correct partition of energy between the fluid and vehicle. This latter problem is most difficult when an Eulerian fluid representation is used.

On the other hand, it is of interest to develop a numerical scheme for the coupled problem when the fluid is in the Eulerian representation, because generalization to three-dimensional sloshing has distinct advantages in the Eulerian representation.

Acknowledgements

The authors are very grateful to both referees for valuable comments which improved the manuscript. Special thanks to the second referee who pointed out that the choice of quadrature formula for σ in Section 6 affects both conservation of symplecticity and conservation of energy.

https://doi.org/10.1017/S0956792510000197 Published online by Cambridge University Press

Appendix A Exact equations based on the average horizontal velocity

In deriving the shallow-water equations in Section 3 the velocity at the free surface is used for the one-dimensional horizontal velocity. There are other possible choices. In this appendix it is shown that another interesting choice is the vertical average of the horizontal velocity. This average is with respect to the full height of the fluid column, from $y=0$ to $y=h$.

When the vertically averaged horizontal velocity

$$\overline{u}(x,t)=\frac{1}{h}\int_0^h u(x,y,t)\,\mathrm{d}y$$

is used then two out of the three equations (3.4)–(3.5) for the coupled problem are exact. Differentiating $h\overline{u}$, using mass conservation, the kinematic free surface condition and the bottom boundary condition, it shows that the equation for h is exact: $h_t+(h\overline{u})_x=0$.

Similarly, the equation for the vehicle motion is also exact since (2.10) is in terms of $\overline{u}$,

$$\frac{\mathrm{d}}{\mathrm{d}t}\left(\int_0^L \rho h\overline{u}\,\mathrm{d}x+(m_f+m_v)\dot{q}\right)=-vq.$$

However, the momentum equation is not exact. Starting with the 2D horizontal and vertical momentum equations (2.1) one can verify by direct calculation that

$$\overline{u}_t+\overline{u}\overline{u}_x+gh_x=-\ddot{q}-\mathsf{Rem},$$

where the remainder has the form

$$\mathsf{Rem}=\frac{1}{h}\frac{\partial}{\partial x}\left[\int_0^h\left(u^2-\overline{u}^2+\int_y^h\frac{Dv}{Dt}\,\mathrm{d}s\right)\mathrm{d}y\right].$$

Hence to use $\overline{u}$ the only assumption required to close the equations is $\|\mathsf{Rem}\|\ll 1$. It is not clear when this term is small, but sufficient conditions are negligible vertical accelerations and $\overline{u}^2\approx u^2$.

Appendix B Variational principle for the coupled system when the fluid motion is Eulerian

The governing equations in the Eulerian representation can also be obtained from a variational principle. Let

$$\mathscr{L}(q,h,U)=\int_0^L\left[\tfrac{1}{2}\rho h(U+\dot{q})^2-\tfrac{1}{2}\rho gh^2+\rho\phi(h_t+(hU)_x)\right]\mathrm{d}x+\tfrac{1}{2}m_v\dot{q}^2-\tfrac{1}{2}vq^2.$$

This Lagrangian functional (for the Eulerian flow field) is of the form

$$\mathscr{L}=KE-PE+\mathsf{constraint},$$

where

$$KE=\int_0^L\tfrac{1}{2}\rho h(U+\dot{q})^2\mathrm{d}x+\tfrac{1}{2}m_v\dot{q}^2\quad\text{and}\quad PE=\tfrac{1}{2}\int_0^L\rho gh^2\,\mathrm{d}x+\tfrac{1}{2}vq^2,$$

https://doi.org/10.1017/S0956792510000197 Published online by Cambridge University Press

with conservation of mass $h_t+(hU)_x=0$ imposed as a constraint. The Lagrange multiplier ϕ is a velocity potential, but since the equations are one-dimensional the potential does not imply potential flow.

Take variations of this Lagrangian:

$$\frac{\partial \mathscr{L}}{\partial \phi}=0 \Rightarrow h_t+(hU)_x=0,$$
$$\frac{\partial \mathscr{L}}{\partial h}=0 \Rightarrow \frac{1}{2}(U+\dot{q})^2-gh-\phi_t-\phi_x U=0,$$
$$\frac{\partial \mathscr{L}}{\partial U}=0 \Rightarrow h(U+\dot{q})-\phi_x h=0,$$
$$\frac{\partial \mathscr{L}}{\partial q}=0 \Rightarrow -\frac{\mathrm{d}}{\mathrm{d}t}\left(\int_0^L \rho h(U+\dot{q})\,\mathrm{d}x\right)-m_v\ddot{q}-vq=0.$$

The first equation is mass conservation. The third equation gives

$$\phi_x=U+\dot{q}.$$

Substitute this expression into the second equation:

$$\phi_t=\tfrac{1}{2}(U+\dot{q})^2-gh-(U+\dot{q})U \quad \Rightarrow \quad \phi_t+\tfrac{1}{2}U^2+gh=\tfrac{1}{2}\dot{q}^2,$$

a form of Bernoulli's equation. Differentiate it

$$\phi_{xt}=(U+\dot{q})U_x-gh_x-UU_x-(U+\dot{q})U_x,$$

which simplifies to

$$U_t+UU_x+gh_x=-\ddot{q},$$

recovering the momentum equation in (3.4). The variation $\partial\mathscr{L}/\partial q=0$ recovers the equation for $q(t)$ in (3.5). However, this variational formulation does not lead to an effective numerical scheme as far as we are aware.

Appendix C Case of spring constant zero

If the spring constant v is zero, then the LPP equation for the vehicle motion (4.2) reduces to

$$\frac{\mathrm{d}^2}{\mathrm{d}t^2}\left(\int_0^L \rho x\chi(a)\,\mathrm{d}a+(m_f+m_v)q\right)=0$$

or

$$\int_0^L x\rho\chi\,\mathrm{d}a+(m_v+m_f)q=\mathsf{c}_1 t+\mathsf{c}_0, \tag{C 1}$$

where c_0 and c_1 are determined by the initial data. In this case the position of the vehicle can be expressed in terms of the fluid motion

$$q(t)=\frac{\mathsf{c}_1}{m_f+m_v}t+\frac{\mathsf{c}_0}{m_f+m_v}-\frac{1}{m_f+m_v}\int_0^L x\rho\chi\,\mathrm{d}a \tag{C 2}$$

https://doi.org/10.1017/S0956792510000197 Published online by Cambridge University Press

with

$$\begin{aligned} \mathsf{c}_1 &= \int_0^L \rho U\,(a,0)\,\mathrm{d}a + (m_f + m_v)\dot{q}(0), \\ \mathsf{c}_0 &= \int_0^L x(a,0)\rho\chi\,\mathrm{d}a + (m_f + m_v)q(0). \end{aligned} \tag{C 3}$$

This result shows that the position of the vehicle $q(t)$ is completely determined by the initial data, and the horizontal component of the centre of mass c.m. of the fluid, since

$$\mathsf{c.m.} = \frac{1}{m_f}\int_0^L \int_0^h \rho x\,\mathrm{d}y\,\mathrm{d}x = \frac{1}{m_f}\int_0^L \rho x h\,\mathrm{d}x = \frac{1}{m_f}\int_0^L x(a,t)\rho\chi(a)\,\mathrm{d}a.$$

References

[1] Alemi Ardakani, H. & Bridges, T. J. (2009a) Shallow-water sloshing in rotating vessels. Part 1: Two-dimensional flow field. URL: `http://personal.maths.surrey.ac.uk/st/T.Bridges/SLOSH/`

[2] Alemi Ardakani, H. & Bridges, T. J. (2009b) Dynamic coupling between shallow-water sloshing and a vehicle undergoing planar rigid-body motion. *Technical Report*, University of Surrey. URL: `http://personal.maths.surrey.ac.uk/st/T.Bridges/SLOSH/`

[3] Alemi Ardakani, H. & Bridges, T. J. (2010) Symplecticity of the Störmer-Verlet algorithm for coupling between the shallow water equations and horizontal vehicle motion. *Technical Report*, University of Surrey. URL: `http://personal.maths.surrey.ac.uk/st/T.Bridges/SLOSH/`

[4] aus der Wiesche, S. (2003) Computational slosh dynamics: Theory and industrial application. *Comput. Mech.* **30**, 374–387.

[5] Bridges, T. J. (2009) Wave breaking and the surface velocity field for three-dimensional water waves. *Nonlinearity* **22**, 947–953.

[6] Caglayan, I. & Storch, R. L. (1982) Stability of fishing vessels with water on deck: a review, *J. Ship Res.* **26**, 106–116.

[7] Chester, W. (1968) Resonant oscillations of water waves. Part I. Theory. *Proc. R. Soc. Lond.* A **306**, 5–22.

[8] Cooker, M. J. (1994) Water waves in a suspended container. *Wave Motion* **20**, 385–395.

[9] Cox, E. A., Gleeson, J. P. & Mortell, M. P. (2005) Nonlinear sloshing and passage through resonance in a shallow water tank. *Z. Angew. Math. Phys.* **56**, 645–680.

[10] Dubois, F., Petit, N. & Rouchon, P. (1999) Motion planning and nonlinear simulations for a tank containing fluid. In: *European Control Conference*, Karlsruhe, Germany, 6 pages.

[11] Feddema, J. T., Dohrmann, C. R., Parker, G. G., Robinett, R. D., Romero, V. J. & Schmitt, D. J. (1997) Control for slosh-free motion of an open container. *IEEE Control Syst. Mag.* **17**, 29–36.

[12] Grundelius, M. & Bernhardsson, B. (1999) Control of liquid slosh in an industrial packaging machine. In: *IEEE International Conference on Control Applications*, Kohala Coast, Hawaii, 6 pages.

[13] Hairer, E., Lubich, C. & Wanner, G. (2003) Geometric numerical integration illustrated by the Störmer-Verlet method. *Acta Numer.* **12**, 399–450.

[14] Ibrahim, R. A. (2005) *Liquid Sloshing Dynamics*, Cambridge University Press.

[15] Ikeda, T. & Nakagawa, N. (1997) Non-linear vibrations of a structure caused by water sloshing in a rectangular tank. *J. Sound Vib.* **201**, 23–41.

[16] Jones, A. F. & Hulme, A. (1987) The hydrodynamics of water on deck. *J. Ship Res.* **31**, 125–135.

https://doi.org/10.1017/S0956792510000197 Published online by Cambridge University Press

[17] Johnson, R. S. (1997) *A Modern Introduction to the Mathematical Theory of Water Waves*, Cambridge University Press.
[18] Leimkuhler, B. & Reich, S. (2004) *Simulating Hamiltonian Dynamics*, Cambridge University Press.
[19] Lui, P.-C. & Lou, Y. K. (1990) Dynamic coupling of a liquid-tank system under transient excitation. *Ocean Eng.* **17**, 263–277.
[20] Marsden, J. E. & West, M. (2001) Discrete mechanics and variational integrators. *Acta Numer.* **10**, 357–514.
[21] Ockendon, J. R. & Ockendon, H. (1973) Resonant surface waves. *J. Fluid Mech.* **59**, 397–413.
[22] Ockendon, H., Ockendon, J. R. & Johnson, A. D. (1986) Resonant sloshing in shallow water. *J. Fluid Mech.* **167**, 465–479.
[23] Oliver, M., West, M. & Wulff, C. (2004) Approximate momentum conservation for spatial semidiscretizations of semilinear wave equations. *Numer. Math.* **97**, 493–535.
[24] Prieur, C. & de Halleux, J. (2004) Stabilization of a 1-D tank containing a fluid modeled by the shallow water equations. *Syst. Control Lett.* **52**, 167–178.
[25] Seymour, B. R. & Mortell, M. P. (1973) Nonlinear resonant oscillations in open tubes. *J. Fluid Mech.* **60**, 733–749.
[26] Tzamtzi, M. P. & Kouvakas, N. D. (2007) Sloshing control in tilting phases of the pouring process. *Int. J. Math. Phys. Eng. Sci.* **1**, 175–182.
[27] Tzamtzi, M. P. & Koumboulis, F. N. (2008) Robustness of a robot control scheme for liquid transfer. In: T. Sobh, K. Elleithy, A. Mahmood & M. A. Karim (editors), *Novel Algortithms and Techniques in Telecommunications, Automation and Industrial Electronics*, Springer-Verlag, Dordrecht, The Netherlands, pp. 156–161.
[28] Verhagen, J. H. G. & van Wijngaarden, L. (1965) Non-linear oscillations of fluid in a container. *J. Fluid Mech.* **22**, 737–751.

https://doi.org/10.1017/S0956792510000197 Published online by Cambridge University Press